Ram pressure stripping made easy: an analytical approach

J. Köppen, P. Jáchym, R. Taylor, J. Palouš

Monthly Notices
of the
ROYAL ASTRONOMICAL SOCIETY

MNRAS **479,** 4367–4390 (2018)
Advance Access publication 2018 June 19

doi:10.1093/mnras/sty1610

Ram pressure stripping made easy: an analytical approach

J. Köppen,[1,2,3]★ P. Jáchym,[1] R. Taylor[1] and J. Palouš[1]

[1]*Astronomical Institute, Czech Academy of Sciences, Boční II 1401, 141 00 Prague, Czech Republic*
[2]*Observatoire Astronomique de Strasbourg, Université de Strasbourg, CNRS, UMR 7750, 11 Rue de l'Université, F-67000 Strasbourg, France*
[3]*Institut für Theoretische Physik und Astrophysik, Universität Kiel, D-24098 Kiel, Germany*

Accepted 2018 June 14. Received 2018 June 14; in original form 2017 November 28

ABSTRACT

The removal of gas by ram pressure stripping of galaxies is treated by a purely kinematic description. The solution has two asymptotic limits: if the duration of the ram pressure pulse exceeds the period of vertical oscillations perpendicular to the galactic plane, the commonly used quasi-static criterion of Gunn and Gott is obtained that uses the maximum ram pressure that the galaxy has experienced along its orbit. For shorter pulses, the outcome depends on the time-integrated ram pressure. This parameter pair fully describes the gas mass fraction that is stripped from a given galaxy. This approach closely reproduces results from smoothed particle hydrodynamics (SPH) simulations. We show that typical galaxies follow a very tight relation in this parameter space corresponding to a pressure pulse length of about 300 Myr. Thus, the Gunn and Gott criterion provides a good description for galaxies in larger clusters. Applying the analytic description to a sample of 232 Virgo galaxies from the GoldMine data base, we show that the intracluster medium provides indeed the ram pressures needed to explain the deficiencies. We also can distinguish current and past strippers, including objects whose stripping state was unknown.

Key words: methods: analytical – galaxies: clusters: general – galaxies: clusters: intracluster medium – galaxies: evolution.

1 INTRODUCTION

In clusters of galaxies, one finds spiral galaxies with a quite normal appearance in the optical region, but whose HI mass is significantly less than expected for a normal spiral of the same type and size. This H I deficiency can be understood as the result of ram pressure stripping from the interaction of the galaxy's interstellar matter (ISM) with the hot intracluster medium (ICM) that fills a cluster and is detected by its X-ray emission, and through which the galaxy travels during its flight in the cluster.

In their study of infall of matter into the centres of clusters of galaxies, Gunn & Gott (1972) estimated that the gas would be removed from a spiral galaxy if the ram pressure exceeded the force density from the galactic disc's gravitational field. Since then ram pressure stripping has been investigated by several numerical techniques (see Schulz & Struck (2001) for an overview of the early work). The smoothed particle hydrodynamics (SPH) simulations by Abadi, Moore & Bower (1999) showed that the stripping radius, i.e. the outer radius of the remnant H I disc, is reasonably well predicted analytically, based on the ideas of Gunn & Gott (1972) using the gravitational attraction of bulge, dark halo, and an infinitesimally thin disc. Vollmer et al. (2001) found that the results of their sticky-particle models could well be matched with the predictions of Gunn & Gott (1972) using the assumption that the maximum restoring force from the potential of bulge, dark halo, and a disc with finite thickness equals the centrifugal force at the stripping radius. Also, fitting formulae were obtained for the fractions of the stripped mass and the reaccreted mass, as a function of maximum ram pressure and tilt angle. The comprehensive 2D hydrodynamical simulations of galaxies subjected to a constant flow of hot ICM by Roediger & Hensler (2005) showed that the stripping radius and stripped mass fractions are a function of ram pressure, but not of ICM density or speed separately. The numerical results could closely be reproduced with the Gunn & Gott (1972) approach by computing the maximum restoring force.

The SPH simulations by Jáchym et al. (2007) cover a wide range of ICM density and spatial extent of the ICM showing how the amount of stripped mass depends on the duration of the pressure pulse. It is found that while the runs with longest pulse durations could be matched by the predictions using the Gunn & Gott (1972) approach, at short pulses stripping relies on the amount of momentum transferred to the galaxy's gas. The tilt angle of the ICM wind plays only a minor role, as long as the angle between the ICM flow direction and normal to the plane of the gas disc is smaller than about 60°, i.e. when stripping occurs nearly face-on (Roediger & Brüggen 2006; Jáchym et al. 2009). The high-resolution three-dimensional hydrodynamical simulations of stripping of galaxies

★ E-mail: koeppen@astrophysik.uni-kiel.de

with a clumpy, multiphase ISM by Tonnesen & Bryan (2009) indicate that low-density gas at any position in the galaxy is quickly removed. High-density clouds are subject to ablation and later are eventually stripped. While it is difficult to quantify how much gas is lost from the disc area inside the stripping radius, this work demonstrates that gas loss from the inner disc might be substantial.

The sticky-particle approach (Vollmer et al. 2001) enabled detailed analyses of a number of H I-deficient galaxies in the Virgo cluster that lead Vollmer (2009) to put them in a sequence beginning from galaxies which just start to be affected by stripping to objects that completed the stripping process and are already past the pressure maximum. In these studies, the observational data must be detailed, such as having HI maps and data cubes in order to match the density and velocity structure of the H I flowing away from the host galaxy. Due to the large computational effort this technique could only be applied for a limited number of the more prominent galaxies.

It would be advantageous to have more efficient techniques requiring less computational modelling that would allow a reliable interpretation based on less detailed data that are available for a larger number of objects. A comparison of SPH simulations (Jáchym et al. 2007, 2009) with analytical considerations showed that the numerical results could be well understood in terms of a substantially simpler kinematical approach. This paper addresses a more complete formulation describing ram pressure stripping which is done by considering the motions of test particles approximating gas parcels of a galaxy in the galaxy's gravitational potential and subjected to an external force pulse.

This analysis allows us to give a comprehensive description how strongly a galaxy is stripped for a given ram pressure history (Section 2). With this analytics we assess the sensitivity of the results on the various parameters of the galaxy (Section 3). This also imposes constraints on the ram pressure histories under which galaxies are stripped (Section 4). Section 5 shows that for the most likely trajectories of a galaxy falling into a cluster centre, the ram pressure histories are well constrained, and that for observed clusters the long-pulse limit is an appropriate approximation. In Section 6, we compare the analytical approach with SPH simulations (Jáchym et al. 2007, 2009) and explore the mass fractions of the stripped gas and of the gas which will fall back onto the disc. In Section 7, we describe our method how to interpret global data from galaxies and apply it to data from the GoldMine data base to identify galaxies which are either currently undergoing stripping or having had a stripping event in the past.

Several interactive JavaScript tools which evaluate the analytical considerations of this paper are available in the internet at http://www.astrophysik.uni-kiel.de/~koeppen/JS/RPShome.html.

2 MOTION OF A GAS PARCEL IN A GALAXY

Let us consider the motion of a parcel of gas in the galactic disc like a single mass point, in the gravitational field of the galaxy and under the influence of an external pressure pulse. Thereby we neglect any internal gas dynamics of the disc and replace the hydrodynamic ISM/ICM interaction by a pressure pulse. In the plane of the disc, this parcel will be at the minimum of the gravitational potential at its distance from the rotational axis. If slightly perturbed in a direction perpendicular to the plane, it will start vertical oscillations of small amplitude. The period of these oscillations depends on the vertical derivative of the force in the galactic plane

$$T_{\rm vert} = 2\pi/\sqrt{\partial^2\Phi(r,z)/\partial z^2|_{z=0}}. \quad (1)$$

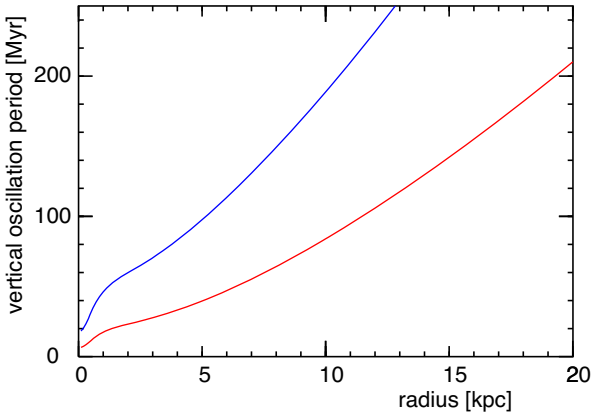

Figure 1. Variation of the period for vertical oscillations about the galactic plane as a function of distance from the centre of a galaxy like the Milky Way (red curve). The blue curve is for NGC 4522 as an example for a smaller galaxy.

For a galaxy similar to the Milky Way, it will vary from around 10 Myr near the centre to 200 Myr near the outer edge, as shown in Fig. 1.

During a stripping event, ram pressure produces an additional force acting on the gas parcel. In the case of face-on stripping, this external force is only in vertical direction with respect to the galactic plane (the x–y plane):

$$\Sigma_{\rm g}\frac{{\rm d}v_x}{{\rm d}t} = -\Sigma_{\rm g}\frac{\partial\Phi}{\partial x}, \quad (2)$$

$$\Sigma_{\rm g}\frac{{\rm d}v_z}{{\rm d}t} = -\Sigma_{\rm g}\frac{\partial\Phi}{\partial y}, \quad (3)$$

$$\Sigma_{\rm g}\frac{{\rm d}v_z}{{\rm d}t} = p(t) - \Sigma_{\rm g}\frac{\partial\Phi}{\partial z}, \quad (4)$$

where equations (2) and (3) define the components in the galaxy's rotational plane and equation (4) gives its component perpendicular to that plane. We assume the surface density $\Sigma_{\rm g}$ of the parcel is specified for a given galactocentric distance r and is constant, i.e. it does not depend on the height z above the galactic plane. The time-varying force $p(t)$ is given by the ram pressure

$$p(t) = \rho_{\rm ICM}(v_{\rm ICM} - v_z)^2, \quad (5)$$

where $\rho_{\rm ICM}$ is the density of the ICM at a place on the galaxy's orbit in the cluster, $v_{\rm ICM}$ is the velocity of the galaxy relative to the ICM and v_z is the velocity of the parcel of gas relative to the parent galaxy. $v_{\rm ICM}$ is of the order of 1000 km s^{-1}, thus well above v_z which is mainly due to the vertical gas motions inside the galaxy (about 10 km s^{-1}) and later eventually increased by the action of ram pressure forces. This means that we may disregard the contribution to the ram pressure due to the galaxy's internal motions.

2.1 Long-pulse limit: the Gunn and Gott criterion

Gunn & Gott (1972) pointed out that gas is held back in the disc of the galaxy, as long as the ram pressure does not exceed the restoring force by the gravitational potential. In the potential of a disc galaxy at some galactocentric distance, the restoring force $\frac{\partial\Phi}{\partial z}(z)$ has a maximum value at some height z above the disc. Taking this as a threshold, the condition of stripping gas from that radius r

is formulated as

$$p_{\rm max} \geq \Sigma_{\rm g}(r) \left| \frac{\partial \Phi(r,z)}{\partial z} \right|_{\rm max} \quad (6)$$

with the maximum ram pressure $p_{\rm max}$ that has occurred so far on the galaxy's orbit in the cluster. The height above the plane at which the maximum restoring force occurs can be obtained from $\partial^2\Phi/\partial z^2 = 0$. In this quasi-static approach, one assumes that the ram pressure increases slowly enough so that the external force remains always balanced by the restoring force and that it lasts until the gas element reaches the height of maximum restoring force. But even if the ram pressure overcomes this maximum, the gas element still remains gravitationally bound to the galaxy. The pressure has to continue until the total energy of the gas element becomes positive and it can escape with its random velocity. This is explored in more detail in Appendix A.

The time it takes the gas element to reach the height of maximum restoring force is of the order of the period for vertical oscillations. Thus, equation (6) forms a criterion for the removal of the gas if the duration of the ram pressure pulse is longer than the period for vertical oscillations. Tests with models for spiral galaxies show that the escape speed at the height of maximum restoring force is still more than 90 per cent of the escape speed in the galactic plane. Thus, the long duration of a force exceeding[1] the maximum restoring force is an essential ingredient of the criterion from Gunn & Gott (1972). We shall name this the long-pulse limit.

As the maximum restoring force decreases outwards in a galactic disc, the gas is lost beyond some radius r where the equality sign holds in equation (6). Thus, the gas disc is truncated at this radius which might be called the *stripping radius*. On its orbit towards the interior of a cluster with its higher ICM density, a galaxy experiences an increasing ram pressure, and the galaxy's gas disc – whose surface density usually decreases outwards – is progressively truncated until some minimum galactocentric radius is reached. As a consequence, the outcome of the stripping event, the gas mass fraction remaining in the disc, depends on the maximum ram pressure that the galaxy had so far been subjected to.

2.2 Short-pulse limit: momentum transfer

At the other extreme end, let us consider a force pulse much shorter than the period for vertical oscillations: As in the classical apparatus of the ballistic galvanometer we may consider the parcel staying at rest in the galactic plane during the duration of the pulse. The parcel of gas with surface density $\Sigma_{\rm g}$ will get all the momentum provided by the pulse, and at the end of the pulse, it will have accumulated the momentum

$$\Sigma_{\rm g} v_{\rm AFTER} = \int p(t)\,{\rm d}t, \quad (7)$$

where $v_{\rm AFTER}$ is the gas parcel's velocity after the pulse. The accumulated momentum is nothing but the ram pressure integrated over the pulse duration. We add the momentum but not the mass of the intracluster medium; the original mass and surface density of the accelerated gas parcel remain constant. This is justified by the fact that the momentum provided by the ICM is connected to the large velocity of the galaxy relative to the ICM, but the ICM density is much smaller than the ISM, thus we may disregard it.

Subsequently, the parcel would perform vertical oscillations whose amplitude depends on $v_{\rm AFTER}$. If this speed exceeds the local escape speed $v_{\rm esc}^2 = -2\Phi$, corrected for the kinetic energy of the parcel's orbital motion

$$v_{\rm AFTER} \geq \sqrt{-2\Phi - v_{\rm circ}^2} \quad (8)$$

the parcel will get stripped. This means that in the short-pulse limit the outcome of a stripping event is determined by the time integral over the ram pressure rather than its maximum value:

$$\int p(t)\,{\rm d}t \geq \Sigma_{\rm g}\sqrt{-2\Phi - v_{\rm circ}^2}. \quad (9)$$

This is quite different from the long-pulse limit. Furthermore, the outcome of a stripping event is independent of the shape of the pressure pulse. The momentum transfer for longer pulses is addressed in more detail in Appendix B. The time-integrated force

$$\begin{aligned} \int p(t)\,{\rm d}t &= \int \rho_{\rm ICM} v_{\rm ICM}^2\,{\rm d}t \equiv (v\Sigma)_{\rm ICM} \\ &\approx \hat{v}_{\rm ICM} \int \rho_{\rm ICM} v_{\rm ICM}\,{\rm d}t = \hat{v}_{\rm ICM}\Sigma_{\rm ICM} \end{aligned} \quad (10)$$

is related to the column density $\Sigma_{\rm ICM}$ intercepted by the parcel during the galaxy's flight through the ICM, as introduced by Jáchym et al. (2007), with the speed $\hat{v}_{\rm ICM}$ of the galaxy near the time of maximum pressure. For convenience, we shall give $(v\Sigma)_{\rm ICM}$ in units of 1000 km s^{-1} M$_\odot$ pc^{-2}.

Table 1. The parameters of the components of the LM4 and LM10 galaxy models: mass inside the truncation radius $r_{\rm trunc}$, radial scale a, and scale height b.

	Mass (M$_\odot$)	$r_{\rm trunc}$ (kpc)	a (kpc)	b (kpc)
Bulge	1.3×10^{10}	4	0.4	–
Stellar disc	6.5×10^{10}	16	4	0.25
LM4: gas disc	6.5×10^{9}	16	4	0.25
LM10: gas disc	6.5×10^{9}	16	10	0.25
Dark halo	3×10^{11}	20	40	–

2.3 The combined diagram

From the two limiting cases it is apparent that there are two parameters, $v\Sigma_{\rm ICM}$ and $p_{\rm max}$, which determine the outcome of a stripping event for a given galaxy. Thus, the diagram of the plane spanned by these two parameters is appropriate for representing the solutions of ram pressure stripping.

A typical spiral galaxy is composed of the stellar bulge, the stellar disc, the gas disc, and the dark matter halo, which form the gravitational potential. Each of the components is described by parameters, e.g. as in Table 1 for models that we use in this paper. Given these properties of a galaxy, the stripped mass fractions can be estimated for any pair $(v\Sigma_{\rm ICM}, p_{\rm max})$: equations (6) and (9) allow us to predict above which radius the gas is removed from the galactic disc. Integration of the gas mass outside this *stripping radius* then gives the stripped mass fraction.

In Fig. 2, we show the predictions for a Milky Way type galaxy (model LM4, with parameters given in Table 1) for stripped mass fractions of 10, 50, and 90 per cent. At 10 per cent stripped fraction only gas from the outer rim of the galaxy is removed, while at

[1] Since the local value of the restoring force decreases beyond the height of this maximum, the ram pressure force needs to be only comparable or can later be even less than the maximum value in order to provide the work necessary for escape.

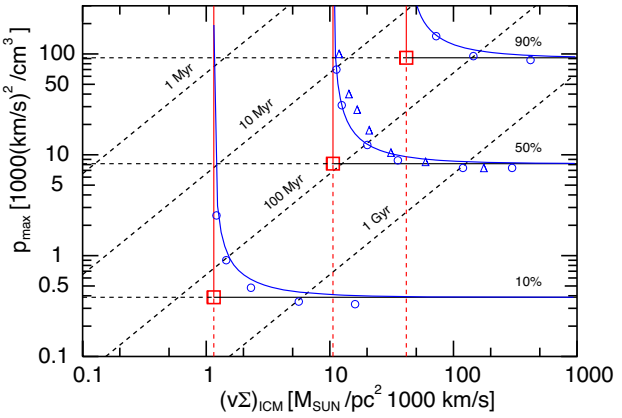

Figure 2. Loci in the plane of maximum p_{max} and time-integrated ram pressure $(v\Sigma)_{ICM}$ predicted for 10, 50, and 90 per cent stripped mass fractions in a Milky Way type galaxy (model LM4 with parameters given in Table 1): The horizontal black line is the long-pulse limit (Gunn & Gott 1972); the vertical red line marks the short-pulse limit. Both are joined with an interpolating curve (in blue). Blue open circles and triangles are results from test particle models that yield the respective stripped mass fractions with Gaussian and Lorentz pulses, respectively. Red squares mark the crossing points of long- and short-pulse limits. Black dashed diagonal lines give the p_{max} versus $(v\Sigma)_{ICM}$ relation for different durations for ram pressure pulse with Gaussian shape.

90 per cent the galaxy is heavily stripped down to its inner parts. The horizontal line is the long-pulse limit (Gunn & Gott 1972), the vertical line marks the short-pulse limit. As a given galaxy can be stripped to the same given level by different combinations of p_{max} and $v\Sigma_{ICM}$ values, i.e. by pulses of different duration and strength – from short/strong to long/weak – the complete geometrical locus for a given stripped fraction is represented by a curve which joins the two limiting cases. A rather simple interpolation is suitable

$$p_{max} = p_0(1 + 0.5/((v\Sigma)_{ICM}/(v\Sigma)_0 - 1)) \quad (11)$$

to provide a smooth transition between the slopes of the two limiting laws. $((v\Sigma)_0, p_0)$ are the coordinates of the crossing point of short- and long-pulse limits that specifies the minimum pulse duration and the minimum peak ram pressure that would be necessary to strip the galaxy to a given stripped mass fraction.

The figure also shows that for a Milky Way type galaxy the criterion of Gunn & Gott (1972) predicts the maximum ram pressure necessary for a certain stripping outcome only if the pulse duration is longer than about 200 Myr for the outer rim (see Fig. 1) and less for the inner parts, i.e. if the time-integrated pressure exceeds a certain value. Shorter pulses require correspondingly higher maximum ram pressures.

Conversely, one may predict which conditions $(v\Sigma_{ICM}, p_{max})$ are necessary for a given galaxy to lose a given fraction of its gas. As these calculations depend on the galaxy's parameters, the position of a stripping event in this diagram gives some information about the galaxy. Regions in the diagram can be identified in which normal galaxies are expected (Section 4).

The diagram has a second aspect: For a given shape of the ram pressure pulse, its time-averaged value and its maximum value completely describe the history of the event. As this history is the result of the galaxy's flight trajectory through the cluster and the distribution of the ICM therein, this diagram can also serve to place constraints on the galaxy's orbit. In Section 6 we identify the regions for most probable orbits in clusters of galaxies.

2.3.1 Test particle models

To allow computation of intermediate cases between the two limits and to facilitate an efficient exploration of how the outcome of stripping events depends on the numerous parameters of the galaxy and the ram pressure history, it is convenient to use numerical models, based on the purely kinematical description of the movement of gas parcels, without any hydrodynamical effects. We consider the evolution of the gas disc in a typical spiral galaxy which is subjected to face-on ram pressure. The time dependence of the ram pressure is modelled as a Gaussian- or Lorentzian-shaped pulse of specified maximum value p_{max} and duration [full width at half-maximum (FWHM)]. The galaxy is composed of bulge, stellar and gas disc, and dark halo, which determine the gravitational potential. As an example, we use the Milky Way-type model LM4 with the parameters given in Table 1. The gas disc is represented by a number (usually 1000) of test particles, each standing for an entire mass ring in the galactic disc. The response to the ram pressure force is followed for each particle by solving its equation of motion in three dimensions (equations 2–4) due to the galaxy's gravitational potential and the ram pressure pulse only. There is no interaction between individual particles. Each particle is given a mass proportional to the surface density at its initial galactocentric radius, and is placed in a circular orbit following the rotation curve. The equations of motion are integrated with a fourth-order symplectic Runge–Kutta type integrator (Forest & Ruth 1990) and adaptive time stepping.

The results match the short-pulse limit quite accurately (Fig. 2), but they require a slightly lower maximum pressure than the long-pulse limit. This is partly because with a constant force the minimum force to dislodge gas parcels is slightly less than the quasi-static estimate, but also because during the long time of the interaction a test particle is pushed by the external pulse from the initial circular orbit into a box orbit, in which it performs oscillations in vertical but also in radial direction. From a more outward position, it is easier to escape. Apart from this small effect, the test particle models demonstrate the validity of the simple interpolating curve between long- and short-pulse limits for both Gaussian- and Lorentzian-shaped pulses.

3 SENSITIVITY OF PARAMETERS

The analytical approach permits us to evaluate more easily the dependence of the expected stripped mass fractions by short- and long-pulses on the numerous parameters of a model galaxy. For some typical examples, we show in Figs 3 and 4 the results for the short- and long-pulse limits. The deficiency $def = \log_{10}(M_0/M) = -\log_{10}(1 - m_{strip})$ is computed from the gas mass M_0 before and after (M) the stripping event, or the stripped mass fraction $m_{strip} = 1 - M/M_0$. Two Milky Way-type galaxy models are shown: The LM4 model [used in the SPH simulations by Jáchym et al. (2007)] is rather resistant to stripping because of its radial scale for the gas had been assumed to be as short (4 kpc) as that of the stellar disc. The LM10 model has a longer gas scale (10 kpc) which is closer to observed HI profiles (Bigiel & Blitz 2012) while having the same total gas mass as LM4. Its lower gas surface density makes the object substantially more vulnerable to ram pressure stripping. To illustrate the effects also on less massive galaxies, we take the example of NGC 4522 that has a rather low rotational velocity near 100 km s^{-1} (Vollmer et al. 2000) that makes it more vulnerable.

The results can be summarized in these terms:

(i) The gravitational potential of the stellar disc strongly influences the galaxy's response to ram pressure stripping. Due to the

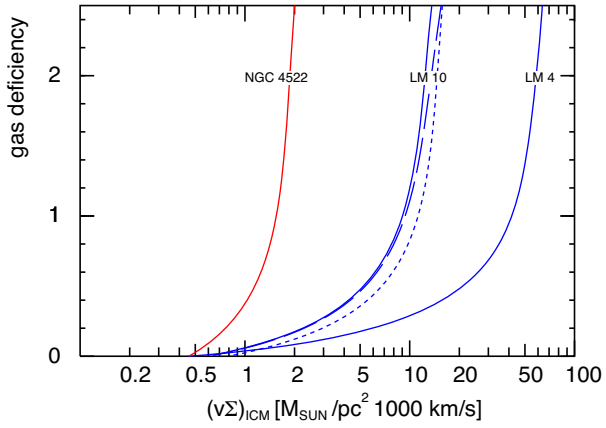

Figure 3. The gas deficiency as a function of the time-integrated ram pressure computed for the short-pulse limit for the Milky Way-like LM4 and LM10 model galaxies and for NGC 4522 (Vollmer et al. 2000). Broken lines refer to the LM10 model with either the bulge (long dashes) or the dark halo (short dashes) mass doubled.

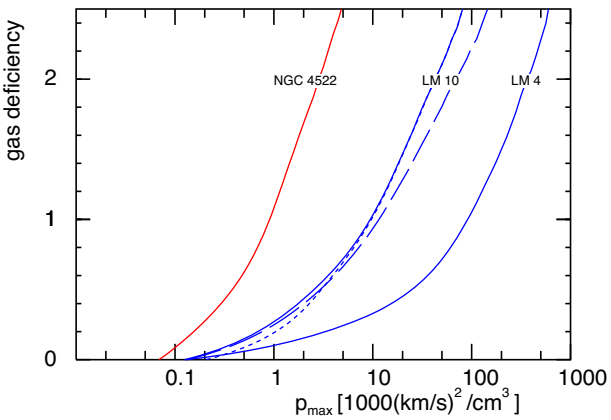

Figure 4. Like Fig. 3, but for the long-pulse limit.

potential's strong variation with height above the plane, it is the dominant factor that controls the vertical restoring force, which in the long-pulse limit must be overcome. The mass of the dark matter halo contributes to the depth of the gravitational potential and hence to the work that must be done by a gas element to escape. However, since the halo contribution has a scale length larger than the thickness of the disc, it does not much affect the vertical restoring force.

(ii) The mass and the radial distribution of gas in the disc are important parameters that determine the outcome of a stripping event. First, the conditions for stripping (equations 9 and 6) depend on the gas surface density at a certain position in the disc. Secondly, they determine the gas mass which is beyond the stripping radius and will be removed.

(iii) The bulge determines the gravitational potential predominantly in the region close to the galactic centre. Thus, its mass and size affect the stripping outcome only in severely and almost completely stripped galaxies.

(iv) The dark matter halo affects mainly the outer parts of the gas disc; hence, it applies mainly to very weakly stripped objects.

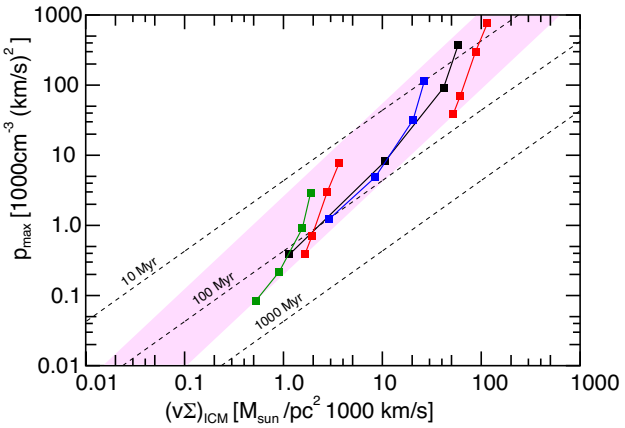

Figure 5. Position of the crossing points of short- and long-pulse limits in the $(v\Sigma)_{\rm ICM}$–$p_{\rm max}$ plane for various models: Black symbols refer to the LM4 galaxy with squares marking stripped mass fractions of 0.1, 0.5, 0.9, and 0.99 (from lower left to upper right). Blue symbols are for NGC 4501 (stellar mass 1.3 10^{11} $M_\odot$), green symbols for NGC 4522 (stellar mass 10^{10} $M_\odot$), using Vollmer's respective mass models. Red symbols are for a nearly flat gas disc (50 kpc radial scale) in the gravitational potential of a stellar disc of 6.5×10^{10} (left) and 6.5×10^{11} $M_\odot$ (right) without bulge or dark halo. The underlying pink area is the region where the crossing points of long- and short-pulse limits of usual galaxies are found. Dashed diagonal lines indicate the durations of the pressure pulse.

4 PREDICTIONS FOR OTHER GALAXIES

The long- and short-pulse limits for a given galaxy to lose a given mass fraction of its gas are described by the maximum ram pressure $p_{\rm max}$ and its time-averaged value $(v\Sigma)_{\rm ICM}$, respectively. Thus, they form two straight lines in the diagram of the $(v\Sigma)_{\rm ICM}$–$p_{\rm max}$ plane. They intersect at some crossing point (see Fig. 2) that can be used to characterize the set of limits. As this position depends on the properties of the galaxy and the given stripped mass fraction, it is of interest to identify which parts of the diagram are accessible for typical galaxies.

When one places a variety of galactic models with realistic parameters and diverse values for the stripped mass fraction in the diagram, it becomes apparent that the positions of the crossing points are confined to a narrow region. In Fig. 2 one notes that the crossing points for the three values of the stripped mass fraction lie on nearly a straight line with a slope somewhat steeper than the lines of equal pulse duration. Since a crossing point describes uniquely the position of its associated curve in this figure, it suffices to display this point in the plane for a given set of galactic parameters and a specified stripped mass fraction, as done in Fig. 5. The black squares – at the same positions as in Fig. 2 – occupy a rather narrow band in the plane, which is shared with galaxies of different parameters.

The position of the crossing point depends strongly on the mass of the galaxy and to a lesser extent on the stripped mass fraction: Red symbols in Fig. 5 pertain to a galaxy model consisting only of a stellar disc with flat rotation curve and a nearly constant-density gas disc (radial scale 50 kpc). A 10-fold increase of the disc mass requires a hundred times greater maximum ram pressure and $(v\Sigma)_{\rm ICM}$ higher by a factor of $10^{1.5}$ to get the same amount of stripping. To increase the stripped mass fraction from 0.1 to 0.99, one needs a 10 times higher $p_{\rm max}$ but only about a factor of 2.5 in $(v\Sigma)_{\rm ICM}$.

The slope of the overall relation $p_{\rm max} \propto (v\Sigma)^{4/3}_{\rm ICM}$ (pink band in Fig. 5) can be understood by using the following approximative relations: The long-pulse limit (equation 6) can be written as

$$p_{\rm max} \approx \Sigma_{\rm g} \frac{v^2_{\rm circ}}{2r} \tag{12}$$

as the maximum restoring force can be approximated by the centrifugal force at the outer radius r of the gas disc (cf. Section 7.1). The short-pulse limit (equation 9) can be written as

$$(v\Sigma)_{\rm ICM} = \Sigma_{\rm g} v_{\rm circ} \sqrt{(v_{\rm esc}/v_{\rm circ})^2 - 1}. \tag{13}$$

As numerical evaluation of the potentials of complete model galaxies (with $v_{\rm circ}(r) \approx$ const.) confirms, we may also assume that $v_{\rm esc}(r) \approx$ const. This yields

$$p_{\rm max} \propto \Sigma_{\rm g} r^{-1}, \tag{14}$$

$$(v\Sigma)_{\rm ICM} \propto \Sigma_{\rm g}. \tag{15}$$

For a weakly stripped galaxy, only the outer parts of the gas disc are affected. Here, the gas surface density profile of a Miyamoto–Nagai disc can be approximated by $\Sigma_{\rm g}(r) \propto r^{-3}$, so that $r \propto \Sigma_{\rm g}^{-1/3}$, giving the simple relation

$$p_{\rm max} \propto (v\Sigma)^{4/3}_{\rm ICM}, \tag{16}$$

which matches the slope of the band depicted in Fig. 5. The band's lower boundary constitutes the limit of negligible stripping. It can be shown that no model with physically sensible parameters can have its crossing point in the region below this boundary line. On the other hand, the upper left-hand area (pulse duration <1 Myr) could only be reached by the crossing points for low-mass gas discs embedded in a very massive potential ($>10^{14}$ M$_\odot$), thus not by typical galaxies.

More complete galaxy models whose rotation curve is computed from the potential of bulge, disc, and dark halo also are restricted to this narrow band, as depicted by the examples for NGCs 4501 and 4522. Since the gas discs are modelled by Miyamoto–Nagai discs with a radial scale of 10 kpc, the variation to cover stripped mass fractions from 0.1 to 0.99 is larger in $(v\Sigma)_{\rm ICM}$ than in constant-density discs. The LM4 model – due to its shorter gas scale of 4 kpc – shows an even larger spread, because of the greater variation of the gas density in the disc.

5 COMPARISON WITH SPH SIMULATIONS

How well does the purely kinematical treatment of the gas in terms of parcels fit to the complex gas dynamics involved in ram pressure stripping of a galaxy? This needs a comparison with numerical models which include the relevant processes in detail. There is no numerical study available that covers a large parameter space suitable for comparison with the analytical predictions in Fig. 2. The closest choice is the SPH simulations by Jáchym et al. (2007) who studied the effects of ram pressure stripping on a Milky Way-like galaxy that radially falls into clusters having a wide range of properties, i.e. the density and the spatial distribution of the ICM.

We briefly summarize the essential details of these simulations. The four components of the galaxy – stellar bulge, stellar disc, gas disc, dark matter halo – are represented with a total number of 42 000 particles, initially distributed in space according to density profiles described in Section 5.2. The ICM is represented by 120 000 SPH particles distributed following the β-profile for a model of the Virgo cluster (Section 5.1). The galaxy starts at rest from the cluster periphery ($R = 1$ Mpc) and freely falls on a radial trajectory towards the cluster centre. In the standard run the galaxy reaches the centre after time $T = 1.64$ Gyr with a velocity of about 1300 km s^{-1}. To treat various cluster environments, the standard values for the ICM of $R_{\rm c,ICM} = 13.4$ kpc and $\rho_{0,\rm ICM} = 6.5\ 10^{-3}$ cm^{-3} are multiplied with factors of 8, 4, 2, 1, 0.5, and 0.25. The standard run yields a maximum ram pressure $p_{\rm max} = 11\,000$ cm^{-3}(km s^{-1})^2 and $(v\Sigma)_{\rm ICM} = 7000$ km s^{-1} M$_\odot$ pc^{-2}.

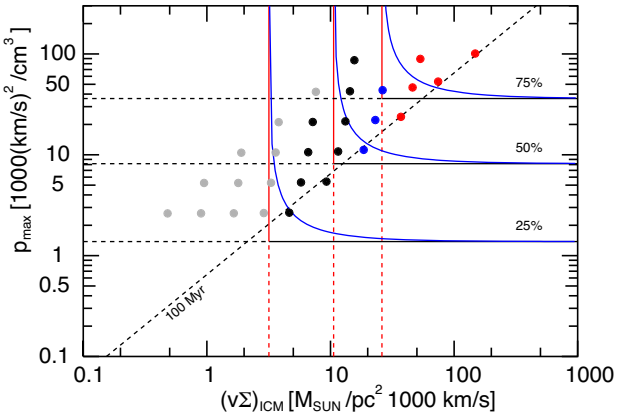

Figure 6. Like Fig. 2, but compared with the results from SPH models (Jáchym et al. 2007) that are shown by large dots whose colour indicates the stripped mass fraction: grey below 0.25, black below 0.5, blue below 0.75, and red above 0.75.

5.1 Cluster model

The Virgo cluster of galaxies is modelled by the distribution of dark matter (DM) and ICM gas. Their volume densities follow β-profiles (Cavaliere & Fusco-Femiano 1976; Schindler, Binggeli & Böhringer 1999; Vollmer et al. 2001): $\rho = \rho_0(1 + R^2/R_{\rm c}^2)^{-3\beta/2}$ with $\beta_{\rm ICM} = 0.47$ and $\rho_{0,\rm ICM} = 0.04$ cm^{-3} $= 4.0\ 10^{-26}$ g cm^{-3} and $R_{\rm c,ICM} = 13.4$ kpc. The dark matter, which provides the gravitational potential, has $\rho_{0,\rm DM} = 3.8 \times 10^{-4}$ M$_\odot$ pc^{-3}, $R_{\rm c,DM} = 320$ kpc, and $\beta_{\rm DM} = 1$.

5.2 Galaxy model

In what follows, we shall focus on a late-type massive galaxy resembling the Milky Way (LM-type in Jáchym et al. (2007)): its model is a four-component system with Plummer spheres for bulge and dark halo and Miyamoto–Nagai discs for stellar and gas discs, with parameters given in Table 1. The resultant rotation curve is flat at about 225 km s^{-1}. We use two versions, LM4 and LM10, which have different radial scales for the gas disc.

5.3 The stripped gas

Fig. 6 shows that the analytical predictions in the $(v\Sigma)_{\rm ICM}$–$p_{\rm max}$ plane agree very well with the results from the SPH simulations. One notes that models with the higher values of $(v\Sigma)_{\rm ICM}$ tend to be more strongly stripped than expected from the analytical considerations. This may indicate that in situations of weak and moderate stripping a kinematic description of the event is well sufficient, but that in longer and more severe interactions, the hydrodynamic aspects become more important.

A more detailed comparison with the predictions from the short-pulse limit (Fig. 7) shows that the SPH results agree very reasonably.

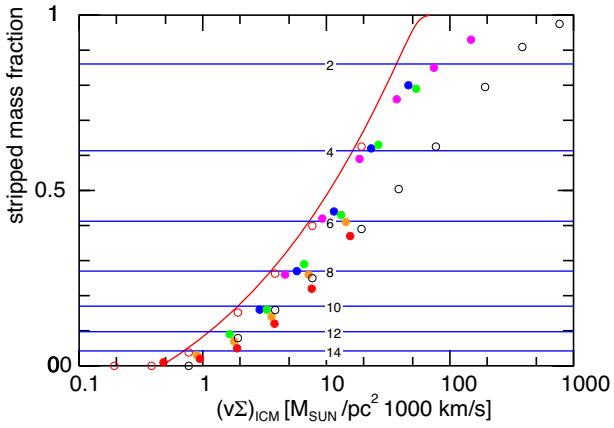

Figure 7. The stripped mass fractions as a function of $(v\Sigma)_{\rm ICM}$ predicted analytically from the short-pulse limit (red curve) compared to the results from the SPH simulations by Jáchym et al. (2007) and Jáchym et al. (2009). The colour of the dots indicates the core radius $R_{\rm c,ICM}$ of the ICM distribution: red, orange, green, blue, and magenta refer to 3.4, 6.7, 13.4, 26.8, and 53.6 kpc that correspond to pulse FWHM durations of 6, 12, 25, 50, and 100 Myr. Small open circles are from test particle models with Gaussian shape force pulses of FWHM durations of 2.5 Myr (red) and 250 Myr (black). Horizontal blue lines indicate the outer radius (in kpc) of the remaining gas disc.

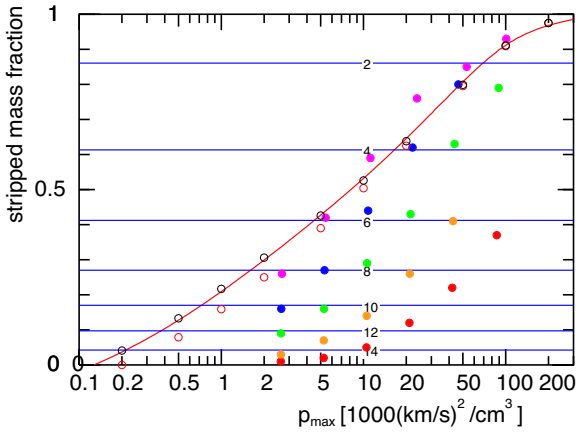

Figure 8. Similar to Fig. 7, but as a function of maximum ram pressure (red curve) predicted for the long-pulse limit. The results from the SPH simulations by Jáchym et al. (2007) are depicted with dots whose colour indicates the core radius $R_{\rm c,ICM}$ of the ICM distribution. The small open circles are test particle models with Gaussian shape force pulses of FWHM durations of 2500 Myr (black) and 250 Myr (red).

However, there is a systematic trend: models with the shortest pulses (6 Myr i.e. $R_{\rm c,ICM} = 3.4$ kpc) are not as strongly stripped as predicted by the short-pulse limit, while those with longer pulses agree better. The SPH results form a rather narrow relation, although their durations cover the range from about 6 to 100 Myr, which would result in a larger spread, judging from the test particle models. This concentration is merely due to a systematic change of the pulse shape in the SPH models: Because of computational economy, the ICM particles had been placed only in a sphere of 140 kpc radius about the cluster centre, as to cover well the principal phase of the stripping. In a small cluster, this would cover indeed a large part of the pressure pulse, which is well approximated by a modified Lorentzian profile ($p(t) \propto (1 + (\Delta t/\tau)^{1.3})$ with the time Δt since maximum pressure and the time-scale τ). But at larger clusters, the pulse is truncated and its core resembles more a Gaussian. As a consequence, the value of $(v\Sigma)_{\rm ICM}$ is reduced by as much as a factor of 0.6 for the largest cluster, shifting the long-pulse points to the left and creating this narrow band.

To show the behaviour close to the long-pulse limit, the stripped fractions are plotted against maximum ram pressure (Fig. 8). As expected, test particle models with pulse durations longer than about 250 Myr match the analytical relation very well, as was already seen in Fig. 6. The SPH simulations with an ICM core radius $R_{\rm c,ICM} > 20$ kpc, which correspond to pulse widths of more than 50 Myr, are still well represented by the long-pulse limit. For $p_{\rm max} = 10\,000{-}50\,000$ cm^{-3}(km s^{-1})^2, the stripped mass fraction exceeds the long-pulse limit. It appears likely that this seeming violation of the long-pulse limit has a similar origin to what is seen in test particle models: due to radial motions gas parcels tend to escape to positions where the gravitational potential is less deep than where the gas had been before the start of the interaction. Other reasons for the deviations between SPH models and the analytical prediction could be that in the SPH simulations the galaxy evolves, forming instabilities and spiral arms, and the hydrodynamics by which one parcel of gas affects its neighbourhood.

In summary, it is remarkable that the purely kinematic considerations alone are capable of predicting stripped mass fractions to within 5 per cent for face-on stripping events for both short and long interactions, despite the apparently large underlying physical differences between SPH simulations and analytical predictions.

5.4 The re-accretable gas

During a stripping event some part of the gas is pushed away from its initial position in the galactic plane, but remains gravitationally bound and will eventually fall back into the disc. In order to distinguish between the gas that is only slightly perturbed and remains close to the galactic plane and the gas that is pushed away from the disc, we shall define the disc as the cylindric volume within 16 kpc galactocentric radius and within $h = 1$ kpc of the plane, similar to Vollmer et al. (2001). Gravitationally bound gas outside this volume is considered as re-accretable gas.

In the short-pulse limit, this relation

$$(v\Sigma)_{\rm ICM} = \int p(t)\,{\rm d}t \geq \Sigma_{\rm g}(r)\sqrt{2(\Phi(r,h) - \Phi(r,0))} \qquad (17)$$

determines the galactocentric distance r outside which gas is kicked out of this volume by an event with given $(v\Sigma)_{\rm ICM}$. Integration from this radius outwards gives the gas mass fraction $m_{\rm kick}$ that also includes the gas that can also escape. The mass fraction that will eventually be re-accreted is $m_{\rm reacc} = m_{\rm kick} - m_{\rm strip}$, with the stripped part $m_{\rm strip}$ computed from equation (9).

The SPH simulations yield somewhat less reaccretable gas than estimated from the analytical arguments (Fig. 9). Test particle models reveal that the reason is the shape of the pressure pulse: While Gaussian pulse models match the analytical predictions very well, modified Lorentzian pulses give smaller reaccretable mass fractions, as do the SPH models.

Fig. 10 shows the situation at maximum pressure for the test particle model equivalent to the standard SPH run. The reaccretable mass extends up to 4 kpc away from the galactic plane, where it joins the material already escaping. After the end of the pressure pulse, this border at 10 kpc galactocentric radius will have further receded to 7 kpc, and the inner border of the kicked material will be at 3.3 kpc radius, as predicted from the short-pulse limit. This

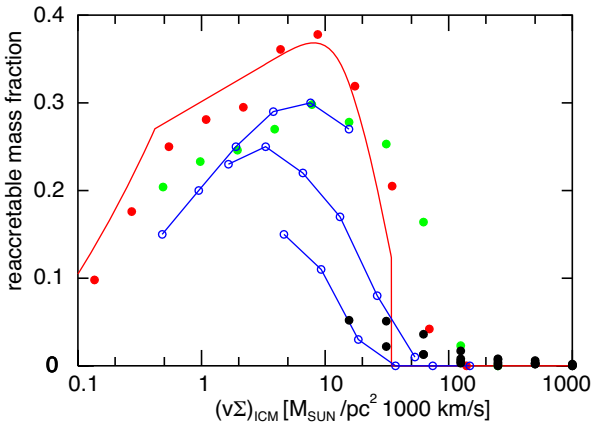

Figure 9. The reaccretable mass fraction as a function of $(v\Sigma)_{\rm ICM}$, as predicted from the short-pulse limit (red curve). SPH models are shown as blue circles, with lines connecting models of the same pulse duration: 6, 25, and 100 Myr (from top to bottom). Test particle models of 6 Myr duration are shown with Gaussian pulse (red dots) and modified Lorentzian pulse (green dots). Black dots pertain to particle models with pulse durations longer than 200 Myr.

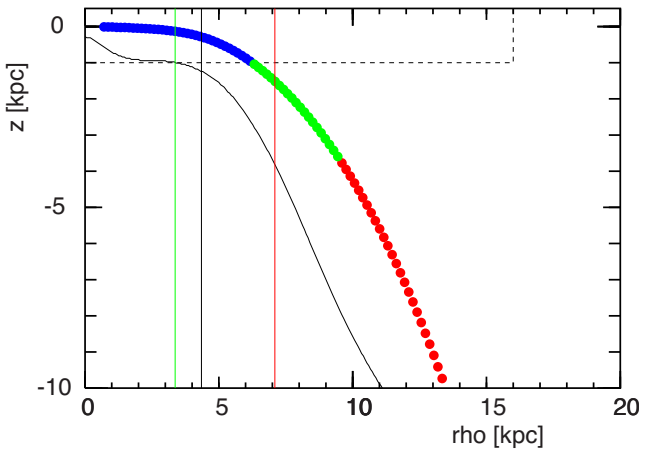

Figure 10. The variation (black curve) of the height of the maximum vertical restoring force with distance from the galactic rotation axis, for the LM4 model. The position of the gas parcels from a test particle model with $R_{\rm c,ICM} = 13.4$ kpc, $\rho_{0,\rm ICM} = 6.5 \times 10^{-3}$ cm^{-3} at the time of maximum ram pressure is shown by coloured dots: blue dots are parcels that remain in the disc (the volume marked by a dashed line); green dots are those kicked out of that volume but remain gravitationally bound to the galaxy; and red dots mark those already escaping. Vertical lines indicate for this standard run the radii outside which gas elements are expected to be stripped in the limits of short (red) and long (black) ram pressure pulses. The green line indicates the radius beyond which gas elements are kicked out of the disc volume, estimated from the short-pulse limit. After the pulse, the green line will indeed form the border between blue and green dots, and the red line will separate green and red dots.

leaves an appreciable mass fraction that will eventually fall back into the disc.

For the outcome in the long-pulse limit, one notes from Fig. 10 that for the LM4 model galaxy the height of peak restoring force is close to 1 kpc for the intermediate part of the disc. This means that once a gas parcel is pushed up to this height, the continued action by the long pulse will drive it into escape. Hence, with our choice for the height of 1 kpc for the disc proper, there will remain no or little reaccretable gas. This is confirmed in the test particle models and SPH models with pulse durations (50 and) 100 Myr and large values of $(v\Sigma)_{\rm ICM}$. SPH models with low values of $(v\Sigma)_{\rm ICM}$ show appreciable reaccretable mass fractions.

6 ORBITS IN CLUSTERS

As discussed in Section 2.3, the stripping outcome for a given galaxy is determined by the position in the $(v\Sigma)_{\rm ICM}$–$p_{\rm max}$ plane. In the idealized situation of a spherically symmetric ICM density distribution about a single cluster centre, the peak ram pressure occurs at the galaxy's closest approach to the cluster centre. The shape of the orbit influences the duration of the pressure pulse. Thus, the position in the $(v\Sigma)_{\rm ICM}$–$p_{\rm max}$ plane is also associated with the parameters of the galaxy's orbit. This allows us to determine which kinds of orbits in a given cluster would be suitable to cause stripping in a given galaxy.

6.1 The most likely trajectories

When a galaxy follows its path through the cluster, the orbit is determined by the cluster's gravitational potential. The maximum ram pressure is reached at the orbit's pericentre and its value is determined from the velocity – hence essentially by the cluster distribution of dark matter – and the local ICM density. The rosette-type orbit can be characterized by the ratio of its apo- to pericentric distances $r_a/r_{\rm p}$ and its closest approach to the centre $r_{\rm p}$. High-resolution cosmological N-body simulations suggest that the orbits of infalling satellite haloes (Wetzel 2011) – cf. the dependence on host halo mass in their fig. 4 – have mostly orbital circularities around 0.5, i.e. an eccentricity of 0.87, which gives an axial ratio $r_a/r_{\rm p} \approx 14$. From their fig. A1, we take that the most likely pericentric distance is $r_{\rm p} \approx 0.2 r_{\rm vir}$ of the virial radius.

6.2 Virgo as an example

Using simple calculations, we explore orbits with parameters $r_a/r_{\rm p}$ and $r_{\rm p}$ from ranges (specified in Fig. 11) that include the most likely values. From each pair of parameters, the initial conditions for the orbit are determined, and the flight of a galaxy through the cluster can numerically be computed, which gives the maximum ram pressure $p_{\rm max}$ and its time integral $(v\Sigma)_{\rm ICM}$. The computation is stopped after its pericentric passage when the galaxy reaches twice the pericentric distance.

Let us consider a galaxy like the Milky Way in the Virgo cluster. With the parameters given in Sections 5.1 and 5.2, one obtains the results presented in Fig. 11. The area in the $(v\Sigma)_{\rm ICM}$–$p_{\rm max}$ plane for models with these orbits is rather small: For the most likely orbits (magenta dots), they cover a range in $(v\Sigma)_{\rm ICM} = 10$–20 and in $p_{\rm max} = 1$–5 in the units of the figure.

The reason for such a concentration of the models is that the duration of the pressure pulse is limited to a rather narrow range: Consider a galaxy on its highly eccentric orbit. The path length on the orbit during which the galaxy is subjected to high ram pressure would be of the order of the pericentric distance. Since its speed will be close to the escape velocity $v_{\rm esc}$ from the cluster centre, the duration of the pressure pulse can be estimated as

$$\Delta t \approx r_{\rm p}/v_{\rm esc} = 0.2 \times r_{\rm vir}/v_{\rm esc} \qquad (18)$$

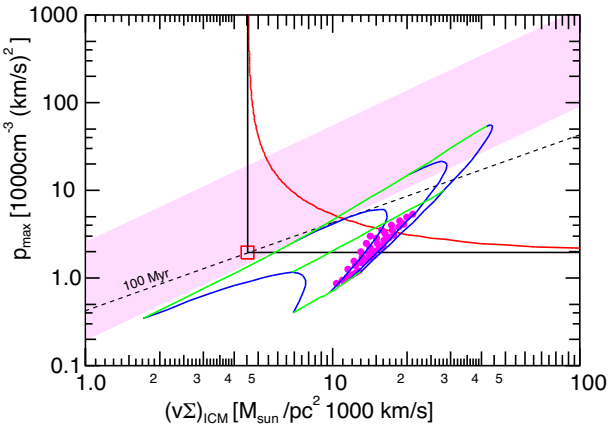

Figure 11. Loci in the plane of maximum p_{max} and time-integrated ram pressure $(v\Sigma)_{ICM}$ predicted for orbits through the Virgo ICM as modelled by Schindler et al. (1999): Green lines mark minimum radii of 0.01, 0.1, and 0.5 Mpc (from top to bottom), blue curves depict $r_a/r_p = 3$, 10, 30, 100 (from left to right). Magenta dots mark the more likely orbits in the range of $7 < r_a/r_p < 28$ and $110 < r_p < 440$ kpc. Horizontal and vertical black lines are the long- and short-pulse limits for the LM10 galaxy model and a stripped mass fraction of 0.5, with the red interpolating curve. As in Fig. 5, the underlying pink area marks the region where the crossing points of long- and short-pulse limits for usual galaxies are found. The diagonal dashed line indicates a pulse duration of 100 Myr.

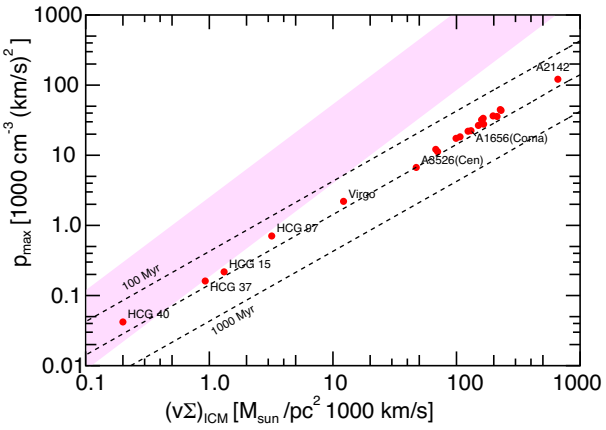

Figure 12. Similar to Fig. 11, but with a dot for the most likely orbit ($r_p = 0.2r_{vir}$, $r_a/r_p = 14$) representing each cluster. Dashed lines indicate the duration of the pressure pulse.

with the cluster's virial radius r_{vir}. The escape speed can be estimated from the cluster mass

$$v_{esc} = \sqrt{\frac{GM}{r_{vir}}} = \sqrt{\frac{4\pi}{3} G\rho_{DM}\, r_{vir}} \tag{19}$$

with the mean dark matter density ρ_{DM}. This results in a pulse duration

$$\Delta t \approx 0.2 \times \sqrt{\frac{3}{4\pi G\rho_{DM}}}, \tag{20}$$

which is a multiple of the free-fall time scale of the cluster.

6.3 Other clusters

The conditions for ram pressure stripping in a cluster can thus be characterized by the most likely orbit, which may be computed from a mass model for the cluster. For a number of galaxy clusters, the X-ray observations have been modelled by Mohr, Mathiesen & Evrard (1999) and Ettori, De Grandi & Molendi (2002), yielding parameters for the distributions of ICM and dark matter. These models show no trend of the mean dark matter density with total mass. Numerical simulations of galactic orbits with $r_p/r_{vir} = 0.2$ and $r_a/r_p = 14$ give FWHM pulse durations in the range of 150–400 Myr with a strong concentration near 200–300 Myr. As a consequence, clusters form a very well-defined relation $p_{max} = 0.2(v\Sigma)_{ICM}$ in the plane of maximum and time-integrated pressure (Fig. 12). The much less massive Hickson compact groups (Rasmussen et al. 2008) have somewhat higher densities and require slightly lower pulse durations, but follow the same relation as massive clusters.

6.4 Implications for galaxies in clusters

Fig. 5 shows that the band to which the crossing points of the short- and long-pulse limits for realistic galaxies are restricted is characterized by pulse durations of less than about 300 Myr. Thus, the conditions for the most likely orbits in clusters (Fig. 12) are found at higher values of $(v\Sigma)_{ICM}$ (for a given maximum ram pressure) than the crossing point that represents the minimum value for $(v\Sigma)_{ICM}$ for the long-pulse limit. Therefore, the long-pulse limit is the more appropriate approximation to explain stripping events in the clusters. However, especially in low-mass clusters and groups, this limit may underestimate the required maximum pressure (cf. Figs. 2 and 11).

The consequences for galaxies can be estimated from Fig. 5: An object like NGC 4501 on the most likely orbit in Virgo (with $p_{max} \approx 2000$ cm^{-3}(km s^{-1})^2) would lose only 10 per cent of its gas, but in the harsher environment of Coma [$p_{max} \approx 20\,000$ cm^{-3}(km s^{-1})^2], it would lose about 90 per cent. A smaller galaxy such as NGC 4522 could lose 90 per cent in Virgo and would be stripped of all its gas in Coma. A galaxy as robust as the LM4 model would attain stripped mass fractions of 0.2, 0.6, and 0.9 in Virgo, Coma, and A2142 ($p_{max} = 100\,000$ cm^{-3}(km s^{-1})^2, respectively.

Since pulse durations are concentrated in the range of 200–300 Myr and since galaxies like the Milky Way have periods for vertical oscillations as long as 100–200 Myr in their outer regions (as seen in Fig. 1), the long-pulse limit may describe weakly stripped galaxies in these cluster less accurately. In situations when the pulse duration is as short as to approach the period for vertical oscillations at the stripping radius, the criterion of Gunn & Gott (1972) would underestimate the ram pressure to cause a given deficiency. This is about a factor of 2 or 3, as shown in the example from Fig. 11.

6.5 Applicability of the short-pulse limit

As we have shown in the previous section, the long-pulse limit provides a good approximation for ram pressure stripping of typical galaxies in most clusters. There may be some situations when galaxies experience effects of short-pressure pulses.

When a galaxy moves with a speed of 1000 km s^{-1} relative to the ambient medium, the encounter with density enhancements smaller than 10 kpc would result in a pulse width of less than 10 Myr. The distribution of ICM in many clusters is far from homogeneous. X-ray observations revealed in the Coma cluster ICM linear structures with a width of 10 kpc (Sanders et al. 2013). Simionescu et al. (2010) identify in Virgo a surface brightness edge as a cold front, i.e. a contact discontinuity associated with gas sloshing in the ICM.

The H I tail left by NGC 4388 (Oosterloo & van Gorkom 2005) has a width between 15 and 40 kpc. Furthermore, there could be hydrodynamical interactions of galaxies: The recent observations of a ram pressure stripped galaxy UGC 6697 and its small companion CGCG 97087N in the Abell 1367 cluster suggest that the small galaxy may have crossed the disc of the main galaxy (Consolandi et al. 2017).

7 COMPARISON WITH OBSERVATIONS: VIRGO CLUSTER

Since our simple, purely kinematical approach is able to reproduce the SPH simulations of ram pressure stripping rather well, we may now attempt to use it to interpret observational data from the Virgo cluster. The aim is to compare the ram pressure that a galaxy might experience at its current position – as estimated from the distribution of the ICM which is known from X-ray observations – to the maximum ram pressure that a galaxy must have undergone, which is obtained from the current state of its gas disc – its HI radius or its H I deficiency. These two pressure estimates should agree in galaxies that undergo active stripping. Galaxies that had experienced stripping long ago would now be in a position where the ICM density is too low to account for their stripping state. This allows us to classify the galaxies, according to their state as *active* and *past strippers*.

While a complete modelling of a stripping event requires the knowledge of numerous parameters that are necessary to describe in detail the galaxy, the cluster, and the galaxy's trajectory through the cluster, it is possible to cut down these requirements substantially.

As shown in Section 6 application of the long-pulse limit appears to be the more appropriate approximation to describe stripping events in galaxies falling into clusters. The criterion of Gunn & Gott (1972) involves only the maximum ram pressure the galaxy has experienced so far, but does not require any information about the detailed time history of the stripping event. As shown by comparison with SPH simulations in a wide range of parameters, application of the analytical criterion for stripping gives reliable estimates for the amount of stripped material. Simulations of various kinds (Vollmer et al. 2001; Roediger & Brüggen 2006; Jáchym et al. 2009) have shown that ram pressure stripping of a tilted galaxy is as effective as in the face-on case, as long as the angle between the flight direction and the normal to the disc is less than about 60°. Thus, an interpretation with the face-on formulae is a reasonable approximation.

Vollmer et al. (2001) pointed out that the results of their simulations of face-on stripped galaxies can well be reproduced by applying the criterion of Gunn & Gott (1972) with the maximum restoring acceleration given by the centrifugal acceleration at the outer rim of its gas disc. In fact, as is shown in Fig. 13 below, the maximum restoring force and the centrifugal acceleration are closely related. As the gravitational potential of spiral galaxies can well be represented by their rotational velocity by assuming a flat rotation curve, a detailed modelling of the potential is not necessary.

The H I gas in spiral galaxies is commonly distributed with a rather flat radial profile, decreasing outwards (Bigiel & Blitz 2012). Hence, reasonable assumptions, such as an exponential disc with a certain radial scale, may be viable.

As only global properties, such as optical radius $r_{\rm opt}$, rotational velocity $v_{\rm rot}$, observed H I mass $M_{\rm H\,I}$, and H I deficiency (in the usual definition as $def = \log_{10}(M_0/M_{\rm H\,I})$ where M_0 is the galaxy's H I mass before stripping) are involved, it is possible to use observational data available for a large number of galaxies. In what follows, this is done for the Virgo cluster with data taken from the GOLDMine data base (Gavazzi et al. (2003), hereafter referred to as GoldMine), which provides homogeneous data for a large number of galaxies. Selecting non-elliptical objects with rotational velocities larger than 30 $\mathrm{km\,s^{-1}}$ yields a sample of 232 objects, of which 197 are H I deficient. Of these are 137 spirals with optical radii between 2 and 20 kpc and 84 dwarf galaxies with radii below about 5 kpc (predominantly of types Im, Sc, Sm, and some BCDs). For 39 larger objects additional information, such as the H I radius, are available from VIVA (Chung et al. 2009). The results from detailed modelling for the objects in various phases of stripping by Vollmer (2009) can serve as a control sample with known stripping properties.

7.1 Assumptions

In both the foregoing analytical considerations and the SPH models, the ISM is treated as a single phase gas, which resembles neutral hydrogen. The comparison with observation also concentrates on the easily observable atomic hydrogen, which provides most of the information about stripped galaxies in the form of the HI deficiency. As the ISM is a complex mixture of neutral, molecular, and ionized phases at various temperatures, the removal of neutral hydrogen from the disc is also influenced by the presence of the other components. Numerical simulations of the response of a multiphase ISM to a stripping event (e.g. Tonnesen & Bryan 2009) show that diffuse H I can easily leave the disc, and HI is also removed by ablation from envelopes of denser clouds that have molecular cores. However, these models do not yet lend themselves to derive generally applicable prescriptions of how the presence of the molecular fraction affects the HI mass-loss. Thus, we may use the empirical approach by Vollmer et al. (2001) who added to the restoring force an enhancement factor that takes into account that in the inner parts of a spiral galaxy the presence of molecular cores make it more difficult to remove neutral hydrogen from gas clouds. The restoring force is multiplied by

$$f = (1 + a\exp(-r_{\rm strip}/R_0)), \tag{21}$$

where $a = 15$ is the enhancement factor and $R_0 = 2$ kpc a radial scale associated with the molecular gas fraction (Vollmer et al. 2001). Thus, the stripping radius $r_{\rm strip}$ – defined as the outer edge of the H I gas that remains gravitationally bound to the galaxy – is determined by the ram pressure p being equal to the maximum restoring force. For a HI gas parcel with surface density $\Sigma_{\rm H\,I}(r)$ at distance r from the centre of the disc, this occurs where this condition holds

$$p = f \times \Sigma_{\rm H\,I}(r_{\rm strip})\left|\frac{\partial\Phi(r,z)}{\partial z}\right|_{\rm max}. \tag{22}$$

If we were to use for galaxies of all sizes the fixed value of the radial scale $R_0 = 2$ kpc, the ram pressure would tend to be overestimated in small galaxies. Chung et al. (2017) find that the diameters of the CO emission are well correlated with the optical diameters, independent of the environment of the galaxies. Their fig. 7 suggests that the majority of their objects has $D_{\rm CO} = 0.75\,D_{\rm opt}$. Therefore, we scale R_0 with the galaxy's optical radius $R_{\rm opt}$:

$$R_0 = 2\,\mathrm{kpc} \times \frac{R_{\rm opt}}{15\,\mathrm{kpc}}. \tag{23}$$

The expression for the stripping radius can be simplified, as the maximum restoring force at some distance but perpendicular to the plane of rotation is closely related to the centrifugal acceleration at this distance. For the gravitational field around a point mass, the ratio g of centrifugal force and maximum restoring force is

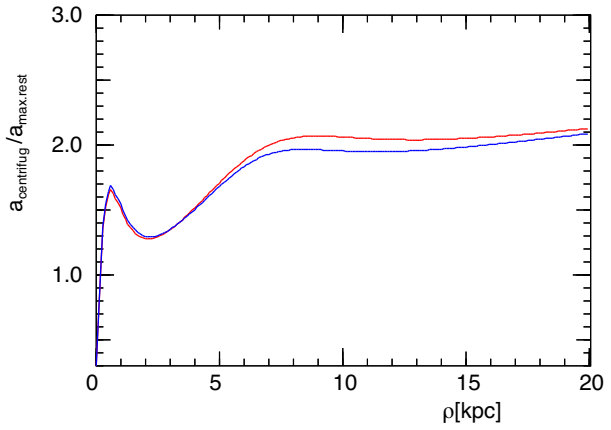

Figure 13. The ratio of centrifugal acceleration and maximum restoring vertical acceleration as a function of distance from the galactic centre in the LM4 model (red, data from Table 1) and the model for NGC 4522 by Vollmer et al. (2000) (blue).

$\sqrt{2}\ 1.5^{3/2} = 2.598$. For Plummer spheres and Miyamoto–Nagai discs, the ratio is zero at the centre and rises to converge to this value for distances larger than the radial scale parameter. In the total gravitational potential of various models for disc galaxies, we find that the ratio in the outer parts always remains nearly constant, as shown in Fig. 13 for two examples. In the following, we adopt the value of $g = 2.0$ for this geometrical factor. Lastly, with a flat rotation curve at speed $v_{\rm rot}$, the centrifugal acceleration at the outer radius $r_{\rm strip}$ of the H I disc is

$$a_{\rm max} = \frac{v_{\rm rot}^2}{r_{\rm strip}}. \tag{24}$$

Thus, a complete description of the gravitational potential of the galaxy is not needed, as it suffices to use the observed value for the rotational speed.

The H I surface density at the stripping radius is obtained from a reasonable guess for the initial spatial distribution of H I in the galaxy. Let the surface density follow a Miyamoto–Nagai profile as a function of the distance r from the galactic centre

$$\Sigma_{\rm HI}(r) = \Sigma_0\,(1 + (r/R)^2)^{-3/2} \tag{25}$$

with its value Σ_0 at the centre and the radial scale R. For an initial outer radius $r_{\rm max,}$ one has

$$\Sigma_0 = \frac{M_0}{2\pi R^2(1 - (1 + (r_{\rm max}/R)^2)^{-1/2})} \tag{26}$$

from the initial mass M_0 in the H I disc, which is computed from the galaxy's present deficiency and HI mass by $M_0 = M_{\rm HI}\,10^{def}$. Other gas distributions, such as an exponential profile, lead to similar expressions. As shown in Fig. C3, the galaxies in the Virgo cluster can be well described by having the H I disc of a radial scale equal to the optical radius $R = r_{\rm opt}$ and an initial outer radius $r_{\rm max} = 1.5R$.

If the stripping radius is known from H I maps (which pertains to the subsample of galaxies in VIVA), a direct estimate for the ram pressure is then obtained from

$$p = \frac{\Sigma_0}{(1 + (r_{\rm strip}/R)^2)^{3/2}}\,\frac{v_{\rm rot}^2}{g\ r_{\rm strip}}\,(1 + a\,e^{-r_{\rm strip}/R_0}). \tag{27}$$

Since this is the maximum value that the galaxy must have experienced so far on its flight through the cluster, we shall name this estimate the *maximum ram pressure* $p_{\rm cfg}$, as it is derived from the centrifugal acceleration.

In most objects of our full sample, the outer radius of the HI disc cannot be measured. But with the same assumptions about the spatial HI distribution, one has

$$10^{-\rm def} = \frac{m(r_{\rm strip})}{m(r_{\rm max})} = \frac{1 - 1/\sqrt{1 + (r_{\rm strip}/R)^2}}{1 - 1/\sqrt{1 + (r_{\rm max}/R)^2}} \tag{28}$$

from which the stripping radius for a given deficiency is obtained. Using this value in equation (27) gives the estimated pressure necessary to produce the deficiency. This estimate we call the *required ram pressure* $p_{\rm def}$.

A comparison with the SPH calculations of Jáchym et al. (2007) shows that for the models with large ICM core radius (53.6 kpc) application of equation (27) (but with $a = 0$) recovers the stripping radius and the maximum ram pressure within 20 per cent.

To facilitate the estimation of ram pressure effects on arbitrary galaxies we have written a few interactive JavaScript tools, at http://www.astrophysik.uni-kiel.de/~koeppen/JS/RPShome.html.

The ICM density at a galaxy's projected position from the cluster centre [from the model of Schindler et al. (1999) with parameters given in Vollmer et al. (2001)], and the local escape velocity (as an estimate of its flight velocity) yields an independent estimate for the actual ram pressure, which we shall name *local ram pressure* $p_{\rm loc}$. As this value is computed for the projected distance from the cluster centre, which is the minimum distance where the galaxy might be, the true local ram pressure would be less for galaxies that lie in the fore- or background in a region of lower density further away from the cluster centre than the projected distance. Since both assumptions are upper limits to the galaxy's speed and the ICM density, the values constitute strict upper limits for the local ram pressure.

7.2 Uncertainties of ram pressure estimates

The estimates $p_{\rm cfg}$, $p_{\rm def}$, and $p_{\rm loc}$ for the ram pressure acting at a galaxy are subject to several uncertainties from measured quantities and from assumptions for the modelling.

For the objects common to VIVA and GoldMine, optical diameters agree within a standard deviation of 0.08 dex, H I masses by 0.1 dex, and widths of the H I line by about 15 km s^{-1}. In this paper, we compute HI deficiencies with the formula from Gavazzi et al. (2013); the values derived by VIVA agree within 0.22 (standard deviation).

VIVA's isophotal H I diameters are within 0.1 dex of the values by Cayatte et al. (1990). This diameter is affected by the presence of extraplanar gas. NGC 4522 is a particularly striking example. The radius at which gas starts to move out of the galactic plane is 3 kpc (Kenney, van Gorkom & Vollmer 2004). With this value, the maximum ram pressure of 1850 cm^{-3}(km s^{-1})^2 is much larger than the local ram pressure of 220 cm^{-3}(km s^{-1})^2. With our modelling of the gas disc, a stripping radius of 4.8 kpc is deduced from the deficiency, yielding a required ram pressure of $p_{\rm def} = 520$ cm^{-3}(km s^{-1})^2.

Rotational velocities are derived from the widths of the H I line, thus they represent the maximum value at the rim of the H I disc. Since in numerous galaxies the rotational velocity still increases with radius – for example NGC 4569 (Guhathakurta et al. 1988; Cortés, Kenney & Hardy 2015) – the derived maximum ram pressures may tend to be overestimated in galaxies whose H I radius is much smaller than its optical radius.

For the estimated ram pressures, one needs to know the HI surface density at the outer edge of the H I disc. Comparison of the values

derived from our modelling of the HI disc and the azimuthally averaged profiles from VIVA suggests that the uncertainties may amount to a factor of 2.

The interpretation of the data by applying the long-pulse limit might lead to systematic underestimation of the ram pressure by a factor of 2–3 (cf. Fig. 11), if the actual pulse length is comparable to the period for vertical oscillations. But as this period is longer in the outer parts of the disc, this underestimation would be restricted to low-deficient objects only. Likewise, the application of the face-on case to objects that undergo tilted ram pressure stripping would lead to systematic underestimation of ram pressure by factors of 2–3 (cf. Jáchym et al. 2007).

In the analysis the ICM is modelled by a smooth and spherically symmetric density distribution centred on M87, while the observed X-ray emission (Böhringer et al. 1994) shows substantial structure, including the presence of a second centre about M49. From their residual map, we estimate variations of up to a factor of 20 in projected density. Shibata et al. (2001) find temperature variations of a factor of 4, on scales larger than about 300 kpc. The density profile is 'very smooth' and well fitted by a single β profile except in the southern region.

Our use of the escape speed considers the limiting case of the infall of galaxies into the cluster occurring on a radial trajectory. But this is not a severe limitation: For the most likely orbit (Wetzel 2011, as discussed in Section 6) with $r_a/r_p \approx 14$, $r_p \approx 0.2 r_{vir}$, and $r_{vir} \approx 1$ Mpc for Virgo, one gets $r_a \approx 3$ Mpc. The maximum speed of this orbit with pericentric distance of 200 kpc is 1700 km s^{-1}, only slightly less than the escape speed of 1770 km s^{-1} from the centre of the β-model to a distance of 3 Mpc. This would reduce the local ram pressure by about 10 per cent.

An important problem is the true distance to individual galaxies, in particular since the Virgo cluster is known to be of triaxial shape (Mei et al. 2007). While for almost all objects we use the distances given by GoldMine (17 Mpc for the main body, 23 and 32 Mpc for the infalling clouds), individual distances have been determined for 11 galaxies by Cortés, Kenney & Hardy (2008) based on the stellar kinematics in the inner 2 kpc. As these values may differ considerably, this affects the linear distance to M87 and hence the deduced local ram pressure. A few typical cases are indicated in Fig. 14below. NGC 4424 is a particularly striking example: GoldMine places it in the 23 Mpc cloud. If this were true and if the 23 Mpc cloud's ICM density were also taken from the model for the main cluster, this galaxy would be classified as a past stripper. But the distance of 15 ± 1.9 Mpc from Cortés et al. (2008) makes it a member of the main cluster, and it counts as an active stripper, where it should belong because of its gas tail (VIVA, Sorgho et al. 2017). Also, four arrows at the bottom of Fig. 14 show by how much the estimated local ram pressure would decrease, if the distance of galaxies at various projected positions would depart by 1 Mpc from the assumed distance of 17 Mpc (from right to left: NGCs 4388, 4405, 4532, and 4808).

Modelling the enhanced retainment of H I by the molecular phase in the inner parts of a galaxy by the enhancement factor from equation (21) adds another uncertainty, since this factor becomes quite important in galaxies with small H I radii, either dwarf galaxies or those with strongly truncated H I discs. The effect of this modelling will be shown in the next section (Fig. 14).

It is rather difficult to assess the total error from these various contributions. Taken all together, we estimate that the accuracy of the pressure values can certainly be not better than a factor of 2.

7.3 Comparison of ram pressure estimates

In this analysis, we compare the local ram pressure p_{loc} provided by the ICM with the pressures that the galaxy must have experienced so far: for objects with measured stripping radius the centrifugal acceleration is used to deduce the maximum ram pressure p_{cfg}. For all galaxies, we also use the measured HI deficiency to deduce the stripping radius and thus derive the required ram pressure p_{def} that accounts for the deficiency. This comparison allows us to distinguish two regimes:

(i) Galaxies whose maximum (or required) ram pressure exceeds the local value are objects that had undergone stripping in the past and are now in a region of low ICM density that would no longer cause any further stripping.

(ii) If the two pressure estimates are comparable, the galaxy is currently undergoing active stripping. Because the local ram pressure is computed with the projected distance from the cluster centre, objects whose local ram pressure is larger than the maximum (or required) ram pressure are likely to be actively stripping, but in the fore- or background.

Let us first consider a subsample of 39 objects from the VIVA catalogue. As these objects have known H I (isophotal) diameters, we can compare the local ram pressure with the *maximum ram pressure* p_{cfg} (computed from equation 27) inferred directly from the centrifugal force at the outer edge of the gas disc.

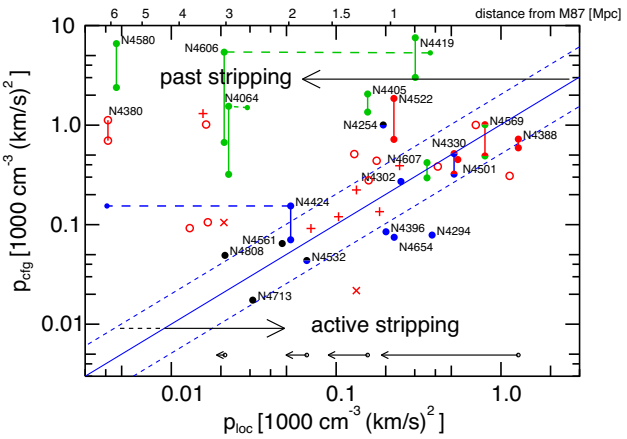

Figure 14. The maximum ram pressure p_{cfg} estimated from the current centrifugal force at the outer rim of the H I discs compared to the local ram pressure p_{loc} obtained from the ICM density at the projected distance from M87 (indicated by the scale at the top) and assuming that the galaxy moves through the ICM with the local escape velocity. The sample comprises only objects with H I isophotal diameter measurements (from VIVA). Red dots mark the sequence of stripped objects (Vollmer 2009), blue dots are galaxies from Chung et al. (2007)(with one-sided H I tails), green dots are galaxies with clearly truncated H I discs, as found by inspection of HI maps in VIVA, and black dots are non-deficient galaxies. Open circles are H I-deficient galaxies ($def > 0.3$), plus signs mark low-deficiency objects ($def < 0.3$), and X-signs are non-deficient objects ($def < 0$), based on the formula of Gavazzi et al. (2013) for deficiency. In several objects, a lower second dot indicates the position if the enhancement factor for the molecular phase is not applied. For NGCs 4424, 4606, and 4064, smaller dots indicate the loci if the distances were taken from GoldMine instead of the individual distances from Cortés et al. (2008). Four arrows at the bottom indicate the decrease of p_{loc} if the distance differed by 1 Mpc from 17 Mpc. The full blue line indicates equality of the pressures; the dashed lines indicate a factor of 2 in either sense.

Fig. 14 shows that near the line of equality one finds galaxies with one-sided tails and extensions (blue dots), which evidently experience ongoing stripping, as well as the galaxies of the sequence of Vollmer (2009) (red dots), which are in stages near maximum ram pressure. Negative deficiency, gas-rich galaxies (black dots) are also found close to the line of equality but at low pressures. Evidently, the conditions at their outer rims are in balance with the local conditions at their large projected distance from M87.

Most galaxies with well-truncated H I discs (green dots), which are a sign for stripping in the past, have indeed maximum pressures larger than the local value. Their projected distances to M87 are above 1 Mpc, thus they appear to be already on their outward journey through the cluster. NGCs 4064, 4293, and 4580 are identified by Yoon et al. (2017) as members of the 'backsplash' population (Gill, Knebe & Gibson 2005). Galaxies that had been stripped on their first passage through the cluster centre and had continued on unperturbed highly eccentric trajectories would now be in the outskirts of the cluster. They could be found either at large projected radii with low line-of-sight speeds (such as NGCs 4064, 4293, 4580, and 4606 with 394, 386, 275, 333 km s^{-1}) or at low projected distances moving nearly parallel along the line of sight with higher speeds (such as NGCs 4419 and 4607 with 1580 and 964 km s^{-1}). Hence, all these objects could be members of the same group.

The application of the pressure enhancement factor (in equation 27) due the molecular gas phase can be quite important in some galaxies. In Fig. 14, the lower dot of several galaxies indicates the value of $p_{\rm cfg}$ when the factor is not applied. The difference is large in galaxies with H I radii less than about 3 kpc. In most galaxies that currently undergo stripping, only those parts are affected that lie well outside the inner region with high molecular content, and hence this factor does not matter.

7.3.1 *The whole sample*

As most of the GoldMine galaxies have no measured H I radius, we now apply to all galaxies the assumptions described in Section 7.1 about the initial H I profile and deduce the current H I radius from present mass and deficiency by equation (28). Then equation (27) gives the estimate for the *required ram pressure* needed to produce the observed deficiency.

In Fig. 15, we compare the required ram pressures with the local ram pressures. The overall picture is very similar to Fig. 14. The required and maximum ram pressures in the subsample of objects with VIVA data agree within a factor of 2. Non-deficient galaxies are absent, because their negative deficiencies would require negative ram pressures. These include NGC 4254 despite its long H I tail. This leaves 197 galaxies.

Vollmer et al. (2001) and subsequent modelling work treat the ISM as a population of H I clouds instead of a smooth gas disc. Appendix D shows that an analytical treatment of this approach yields very similar results, albeit giving systematically higher required ram pressures that are somewhat below the pressures used in the individual modellings by Vollmer.

7.3.2 *Catalogue of galaxies with active and past stripping*

These results allow us to identify in the GoldMine sample all objects near and below the line of equality as candidates for undergoing stripping at the present time, while those well above the line with $p_{\rm def} > 2p_{\rm loc}$ are candidates that were stripped in the past. Since the accuracy of the ram pressures estimates will not be better than about

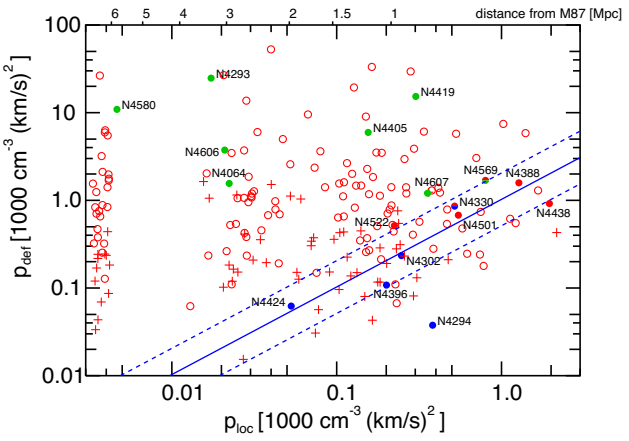

Figure 15. Similar to Fig. 14, but for the ram pressures computed from the deficiency and assuming that the H I disc follows a Miyamoto–Nagai profile with radial scale equal to the optical radius. This comprises the entire sample taken from GoldMine. The group of objects at very low local ram pressure are galaxies of the 23 Mpc cloud, computed under the assumption if the ICM model for the main cluster were extrapolated to that distance.

a factor of 2, objects near the line of equality can be of either type. Choosing the upper line in the figure as the border between the types gives some preference to pick galaxies actively subject to stripping. Tables E1 and E2 list these two groups of objects, whose inclination-corrected rotational velocities are above 30 km s^{-1}. Among the 50 galaxies with active stripping (also including NGC 4522) are 23 low-deficiency objects ($def < 0.3$); 147 objects must have had stripping in the past, including 16 low-deficiency galaxies. A further 35 non-deficient galaxies ($def \leq 0$; not displayed in Fig. 15; Table E3) complete our sample.

Except for the 39 objects in common with VIVA, the majority of the entire sample lacks H I maps, which is indicated in the tables as the absence of an entry for the isophotal H I radius from VIVA. Thus, among high-deficiency objects in Table E1, one finds 19 candidates with active stripping: NGCs 4413, 4438, and 4540, ICs 797, 3059, 3142, 3105, 3239, 3258, 3311, 3365, 3414, 3453, 3476, 3583, and 3611, and VCCs 328, 1605, and 1644. They are rather small with optical diameters between 1 and 3 arcmin and are between 1 and 6 deg of M87. High-resolution H I maps of these galaxies might very likely show direct signs for the ICM–ISM interaction, such as HI discs with extensions and asymmetries. Likewise, one could expect that the 85 high-deficient objects with past stripping would show well-truncated HI discs.

7.3.3 *Interpretation of the* $p_{loc}-p_{cfg}$ *diagram*

In the idealized case of the long-pulse limit, a galaxy has always time to fully respond to the external ram pressure $p_{\rm loc}$, given by the density of the ICM at the distance from the cluster centre and the galaxy's speed. Therefore, the HI disc will always be stripped to the stripping radius, where the external ram pressure is balanced by the galaxy's restoring force. Thus, the maximum ram pressure $p_{\rm cfg}$ estimated from the outer rim of the H I disc is equal to the external ram pressure.

During the infall of a galaxy into the cluster, the external ram pressure $p_{\rm loc}$ first increases with time, then reaches a peak value at the closest approach to the cluster centre, and finally decreases again. Consequently, $p_{\rm cfg}$ first follows $p_{\rm loc}$ closely, up to the moment of peak pressure at pericentric distance. After that $p_{\rm loc}$ decreases,

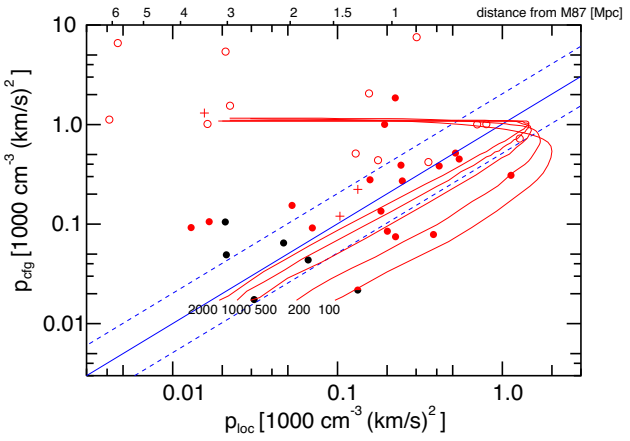

Figure 16. Like Fig. 14, but red dots mark galaxies that show extra-planar gas, one-sided extension of the disc, or asymmetric morphology in VIVA's HI maps. Black dots indicate non-deficient galaxies. For the mass model of NGC 4522 (Vollmer et al. 2006), evolutionary tracks are computed from test particle models with Lorentzian pulses of various FWHM durations (as indicated in Myr). The track for the longest pulse has a maximum ram pressure of 1400 cm^{-3} (km s^{-1})^2; for shorter pulses the pressure is raised to give the same stripped mass fraction of about 0.9, i.e. $def = 1$.

while p_{cfg} remains constant as there will be no further stripping. This produces a very simple evolutionary track in the (p_{loc}, p_{cfg}) diagram: The first part follows the line of equality up to the position of peak pressure, and is independent of the orbital parameters and the properties of the galaxy. The second part at constant p_{cfg} is determined by the peak pressure at pericentric distance.

Since such an evolutionary track is determined only by the ram pressure history, it can be computed by test particle models (as in Section 2.3.1) where a galaxy is subjected to a ram pressure pulse. The tracks in Fig. 16 are computed for the mass model of NGC 4522 (Vollmer et al. 2006) and pressure pulses with Lorentz profile of various durations. While the conditions at pericentric distance determine the maximum ram pressure, the orbit's eccentricity determines the pulse duration. The peak pressure for the longest pulses is 1400 cm^{-3}(km s^{-1})^2, which corresponds to a pericentric distance of about 0.35 Mpc. The galaxy's gravitational restoring force also includes the enhancement factor due to the molecular phase.

In Fig. 16, the VIVA sample is shown in a plot similar to Fig. 14 but emphasizing the galaxies with H I tails, extraplanar gas, or any clear asymmetry in their H I distribution. The figure shows that for pulse durations longer than 1000 Myr – which amounts to five periods for vertical oscillations in the outer parts of the galaxy (cf. Fig.1) – the tracks follow the line of equality and have a sharp turn into the horizontal part at peak ram pressure. As they are within a factor of 2 of the equality $p_{cfg} = p_{loc}$, the maximum pressure p_{cfg} deduced from the stripping radius is indeed a good measure of the actual ram pressure. The break point between diagonal and horizontal tracks does not coincide exactly with the condition $p_{cfg} = p_{loc}$. This is due to deviations of the rotation curve of the model for NGC 4522 from a constant speed, which is supposed in the computation of p_{cfg} and the radial dependence of the vertical oscillation period.

Shorter pulses give substantial deviations from the equal pressure line. At typical pulse widths of 300 Myr (cf. Fig. 12, and as found by Vollmer from detailed modellings), the inferred maximum pressure p_{cfg} tends to underestimate the true ram pressure at that instant. Furthermore, at the time of peak pressure the deduced maximum pressure still remains below its terminal value: in short-pulse stripping events a substantial amount of the gas removal occurs only *after* the peak ram pressure, as gas parcels are first pushed away from the galactic plane but then require more work and time to escape.

Given the diverse uncertainties involved in the ram pressure estimates, discussed in Section 7.2, it is quite remarkable how well the galaxies of different H I morphologies occupy different regions in this diagram: objects with signatures of ongoing stripping such as H I extensions are close to the line of equality, and galaxies with well-truncated discs tend to have large distances from the cluster centre. Non-deficient galaxies are found near the line of quality, with low inferred ram pressures and at large distances from the centre. This suggests that they could be galaxies at the start of their infall into the cluster, during which they become active strippers, and after passage close to the centre to become highly deficient objects with well-truncated HI disc and to emerge again to large distance from the centre. This is consistent with the findings by Yoon et al. (2017).

8 CONCLUSIONS

Ram pressure stripping is thought to be the dominant gas removal mechanism for galaxies in clusters. A full treatment of this process requires hydrodynamic numerical simulations employing complex and detailed physics (such as heating from the ICM, gas cooling by various processes, and stellar feedback). The often used criterion by Gunn & Gott (1972) provides a very convenient analytic approximation from which the amount of stripped gas can be estimated. We have extended this quasi-static criterion to ram pressure pulses of arbitrary duration.

A galaxy falling into a cluster moves on a highly eccentric trajectory through the ICM and experiences a ram pressure that increases as it approaches the inner cluster with the denser ICM. At the closest distance to the cluster centre, the ram pressure reaches a peak value, and on the way out, the pressure decreases again. Thus, the ram pressure is a pulse (of e.g. Lorentz profile) characterized by a maximum value and duration. We consider the motion of gas parcels in the galaxy's gravitational field and under the influence of this pressure pulse. We find that the outcome of a stripping event – the amount of stripped gas and the stripping radius – is determined by the duration of the pressure pulse in relation to the period for oscillations perpendicular to the plane:

(i) With long pulses, one approaches the criterion of Gunn & Gott (1972), where the outcome depends on the maximum ram pressure p_{max}.

(ii) For short pulses, the outcome depends on the time-integrated ram pressure $(v\Sigma)_{ICM}$, because the acceleration of gas parcels is governed by momentum transfer.

With these two limiting cases a comprehensive analytic description is provided for the results of stripping due to pressure pulses of any duration and shape. For a galaxy, the amount of stripped gas can be estimated from the ram pressure history and vice versa.

Simple numerical models, based on this kinematical treatment of the motion of gas parcels in the gravitational field of a galaxy, give a very good agreement with the results of the SPH simulations of Jáchym et al. (2007, 2009), which treat the dynamics of the gas more accurately. Thus, it is possible to reliably estimate for the face-on stripping situation how much gas is removed from the galaxy for good and also how much is only pushed out of the plane but will eventually fall back into the disc. Likewise, the radii beyond which gas escapes or is only pushed away from the plane can be predicted. That purely kinematic arguments suffice to provide a

good approximation indicates that for these quantities more intricate details of fluid dynamics do not play a major role.

In normal galaxies, the periods for vertical oscillations about the galactic plane range between 50 and 200 Myr. This restricts the validity for the long-pulse limit, namely the criterion of Gunn & Gott (1972) to stripping events that are substantially longer than these values. If the pulse duration is so short as to approach the period for vertical oscillations, the criterion tends to underestimate the maximum ram pressure needed for a given deficiency. This is an important caveat that must be kept in mind when using the criterion of Gunn & Gott (1972).

Cosmological *N*-body simulations suggest that the most likely orbits of infalling satellites are highly eccentric and reach pericentric distances of 20 per cent of the virial radius. From the distributions of ICM and dark matter in clusters, deduced from X-ray observations, we find that in a wide range of clusters the typical pulse widths are concentrated around about 300 Myr. This implies that

(i) In massive clusters, the long-pulse limit is the more appropriate approximation for the interpretation of stripping events. Deficiency and stripping radius are determined by the peak ram pressure encountered by a galaxy.

(ii) In less massive clusters and groups, the transfer of momentum becomes increasingly important. Thus, the application of the quasi-static criterion of Gunn & Gott (1972) will tend to underestimate the necessary ram pressures.

Together with reasonable approximations for spiral galaxies (flat rotation curve, initial parameters of the H I gas disc, centrifugal acceleration as proxy for the maximum restoring force, correction for the presence of molecular gas), the long-pulse limit can be used to analyse observations of galaxies in large samples with limited knowledge of their gas content or surrounding ICM conditions. Only a very few observational parameters are required: present HI mass, H I deficiency, optical diameter, and rotational velocity. Application of this analytic method to the deficient galaxies of the Virgo cluster shows that in galaxies with clear signs for ongoing stripping the ram pressure required for the measured deficiencies matches well with the value estimated from the ICM density and the estimated flight speed. The comparison of these two pressure estimates then allows us to identify active and past strippers among galaxies whose stripping phase had not yet been determined. Our analysis has identified 19 highly H I-deficient galaxies not previously mapped by VIVA that are clear candidates for active stripping. Interferometric HI imaging could reveal direct signs of the ongoing ICM–ISM interaction. Furthermore, in 85 past strippers one expects clearly truncated HI discs.

ACKNOWLEDGEMENTS

Hearty thanks go to Richard Wünsch who asked a question which turned out to be the clue to the complete solution. This research has made use of the GOLDMine Database operated by the Universita' degli Studi di Milano-Bicocca. We gratefully acknowledge support by the grant project 15-06012S of the Czech Science Foundation, the project LM2015067 of the Ministry of Education, Youth and Sports of the Czech Republic, the institutional research project RVO:67985815., the Albert Einstein Center for Gravitation and Astrophysics via the Czech Science Foundation Project 14-37086G. We thank Edmunds Optics whose catalogue slogan provided an inspiration for the title.

REFERENCES

Abadi M. G., Moore B., Bower R. G., 1999, MNRAS, 308, 947
Bigiel F., Blitz L., 2012, ApJ, 756, 183
Böhringer H., Briel U. G., Schwarz R. A., Voges W., Hartner G., Trümper J., 1994, Nature, 368, 828
Broeils A. H., Rhee M.-H., 1997, A&A, 324, 877
Cavaliere A., Fusco-Femiano R., 1976, A&A, 49, 137
Cayatte V., Van Gorkom J. H., Balkowski C., Kotany C., 1990, AJ, 100, 604
Chung A., van Gorkom J. H., Kenney J. D. P., Vollmer B., 2007, ApJ, 659, L115
Chung A., van Gorkom J. H., Kenney J. D. P., Crowl H., Vollmer B., 2009, AJ, 138, 1741 (VIVA)
Chung E. J., Yun M. S., Verheijen M. A. W., Chung A., 2017, ApJ, 843, 50 (CO)
Consolandi G., Gavazzi G., Fossati M., Fumagalli M., Boselli A., Yagi M., Yoshida M., 2017, A&A, 606, A83
Cortés J. R., Kenney J. D. P., Hardy E., 2008, ApJ, 683, 78
Cortés J. R., Kenney J. D. P., Hardy E., 2015, ApJS, 219, 9
Damas-Segovia A. et al., 2016, ApJ, 824, 30
Ettori S., De Grandi S., Molendi S., 2002, A&A, 391, 841
Forest E., Ruth R. D., 1990, Physica D, 43, 105
Gavazzi G., Boselli A., Donati A., Franzetti P., Scodeggio M., 2003, A&A, 400, 451 (GoldMine)
Gavazzi G., Fumagalli M., Fossati M., Galardo V., Grossetti F., Boselli A., Giovanelli R., Haynes M. P., 2013, A&A, 553, A89
Gill S. P. D., Knebe A., Gibson B. K., 2005, MNRAS, 356, 1327
Guhathakurta P., van Gorkom J. H., Kotanyi C. G., Balkowski C., 1988, AJ, 96, 851
Gunn J. E., Gott R. J., , III, 1972, ApJ, 176, 1
Jáchym P., Palouš J., Köppen J., Combes F., 2007, A&A, 472, 5
Jáchym P., Köppen J., Palouš J., Combes F., 2009, A&A, 500, 693
Kenney J. D. P., van Gorkom J. H., Vollmer B., 2004, AJ, 127, 3361
Mei S. et al., 2007, ApJ, 655, 144
Mohr J. J., Mathiesen B., Evrard A. E., 1999, ApJ, 517, 627
Oosterloo T., van Gorkom J., 2005, A&A, 437, L19
Rasmussen J., Ponman T. J., Verdes-Montenegro V., Yun M. S., Borthakur S., 2008, MNRAS, 388, 1245
Roediger E., Brüggen M., 2006, MNRAS, 369, 567
Roediger E., Hensler G., 2005, A&A, 433, 875
Sanders J. S., Fabian A. C., Churazov E., Schenkochihin A. A., Simionescu A., Walker S. A., Werner N., 2013, Science, 341, 1365
Schindler S., Binggeli B., Böhringer H., 1999, A&A, 343, 430
Schulz S., Struck C., 2001, MNRAS, 328, 185
Shibata R., Matsushita K., Yamasaki N. Y., Ohashi T., Ishida M., Kikuchi K., Böhringer H., Matsumoto H., 2001, ApJ, 549, 228
Simionescu A., Werner N., Forman W. R., Miller E. D., Takei Y., Böhringer H., Churazov E., Nulsen P. E. J., 2010, MNRAS, 405, 91
Sorgho A., Hess K., Carignan C., Oosterloo T. A., 2017, MNRAS, 464, 530
Tonnesen S., Bryan G. L., 2009, ApJ, 694, 789
Vollmer B., 2009, A&A, 502, 417
Vollmer B., Huchtmeier W., 2003, A&A, 406, 427
Vollmer B., Marcello M., Amram P., Balkowski C., Cayatte V., Garrido O., 2000, A&A, 364, 532
Vollmer B., Cayatte V., Balkowski C., Duschl W. J., 2001, ApJ, 571, 708
Vollmer B., Soida M., Otmianowska-Mazur K., Kenney J. D. P., van Gorkom J. H., Beck R., 2006, A&A, 453, 883
Wetzel A. R., 2011, MNRAS, 412, 49
Yoon H., Chung A., Smith R., Jaffé Y. L., 2017, ApJ, 838, 81

APPENDIX A: LONG PULSE LIMIT

The basic response of a gas element to ram pressure is well illustrated by a simple model: A particle initially at rest at the centre of the potential $\Phi(z) = -0.5/(1 + z^2)$, with the height z above the galactic plane, is subjected to a pulse of external force. Using scaled units in which the escape speed from the centre is unity, the period

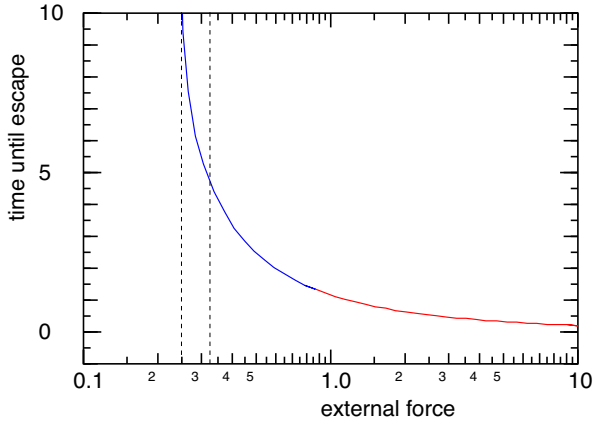

Figure A1. The times for a particle to escape from the potential well as a function of the external force, which rises at time zero rapidly like $(1 - \exp(-t/\tau))$ with $\tau = 0.1$ to a constant value. In the red part of the curve, the particle attains positive total energy before reaching the height of maximum restoring force; in the blue part, it is accelerated to escape speed only after passing that height. The right vertical dashed line indicates the maximum restoring force; the left vertical one marks the minimum value for a constant force necessary to cause escape.

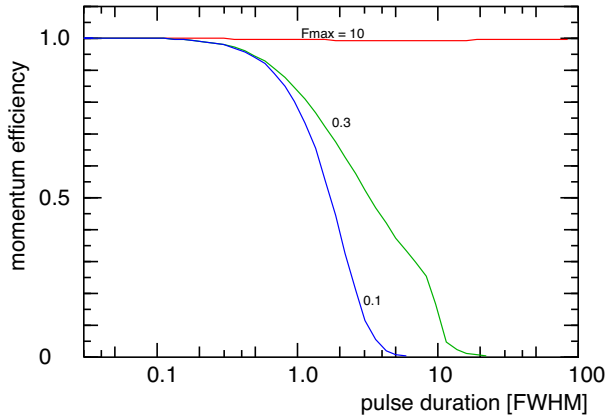

Figure B1. The fraction of the momentum deposited on a test particle in a schematic potential well which is subjected to a Gaussian force pulse with peak value $F_{\max}$ and various FWHM durations. The minimum force to overcome the well's restoring force is 0.3247, and the period for small oscillations about the rest position is 2π, in the normalized units of the model. The red curve is for cases where the particle escapes from the well; for the green and blue curves, the particle remains bound, but is perturbed by the force pulse to oscillate about the rest position.

for oscillations about the rest position is 2π. The maximum restoring force occurs at $z = 1/\sqrt{3} = 0.577$ and is 0.3247 in these units. Since the potential at that point is $-3/8$, the particle still remains gravitationally bound. In order to escape it must thus either have already sufficient speed at this height or need further acceleration by a continuing external force.

For a constant force, Fig. A1 shows that the time until the particle escapes decreases with higher force: For a strong force (more than about thrice the maximum restoring force) the particle's total energy becomes positive even before the particle reaches the height of maximum restoring force. It thus is quickly dislodged. If the force is less than this value, the particle needs some time – of the order of a quarter period of vertical oscillations: about 1.5 time units – to reach the height for maximum restoring force. Thereafter it receives the acceleration to escape speed by the continuing external force, for which a smaller but longer force pulse is sufficient.

The galaxy's orbit and the ICM distribution determine the height and duration of the ram pressure pulse. Using various pulse forms different galaxies exhibit a similar general behaviour to that depicted in Fig. A1. The minimum ram pressure necessary to dislodge a gas parcel is influenced somewhat by the shape and duration of the ram pressure pulse: for this simple model the quasi-static estimate is $F_{\min} = 0.3247$, with a constant force it can be shown to be 0.25, for Gaussian and Lorentzian pulses one gets 0.35 and higher values for shorter pulses. But as these values are quite close, one may well use the more convenient quasi-static formulation.

APPENDIX B: EFFICIENCY OF MOMENTUM TRANSFER

If the pressure pulse is much shorter than the period of vertical oscillation, the gas element acquires the full momentum $(v\Sigma)_{\rm ICM}$ imparted to it and behaves accordingly, as described by the short-pulse limit. What happens for longer pulse durations can be understood in the mechanical analogy of a spring balance: When it is compressed by a slowly increasing external force – this corresponds to the slow increase of the ram pressure during the galaxy's flight towards the cluster centre – its deflection from the resting position will faithfully reproduce the static force-deflection relation $F(z) = -Dz$. This pertains as long as the force does not exceed some limit value for its elasticity, which corresponds to the maximum value of the restoring force in a galactic disc. When the force slowly subsides, the balance will return to its rest position, again following the force–deflection relation. Thus, a slow and long pulse will not have any effect apart from pushing temporarily the gas away from its rest position. However, the momentum provided ($\int F(t)\mathrm{d}t$) does not include the work done against the spring during compression or obtained from it during release:

$$F(t) = m\dot{v} - Dz, \tag{B1}$$

$$\int F(t)\,\mathrm{d}t = m\Delta v - D\int z(t)\,\mathrm{d}t. \tag{B2}$$

Thus, the ratio of the momentum deposited $m\Delta v$ and the momentum provided ($\int F(t)\mathrm{d}t$) describes to what extent momentum transfer is involved in the interaction. Let us call this ratio *momentum efficiency*.

The dependence of this quantity on the duration of the pressure pulse is summarized in Fig. B1, for the simplified model (as in Appendix A) of a particle initially at rest at the bottom of a potential $\Phi(z) = -0.5/(1 + z^2)$, then subjected to a Gaussian force pulse with FWHM duration δ and maximum height $(1 + \delta)/\delta$. The simulation covers the time from 3δ before the peak force to 3δ after it.

If the pulse is strong enough to make the particle escape, all the provided momentum is deposited in the particle, independent of pulse duration or shape.

For weaker pulses the particle remains in the potential well, but the outcome depends on the duration of the pulse: In short pulses, all the momentum is deposited in the particle, which then oscillates about the rest position with a period of 2π in the scaled units of the model and an amplitude corresponding to the deposited momentum. If the pulse is longer than this characteristic period, the particle is merely displaced from the rest position and then brought back, without any momentum remaining. The green curve in Fig. B1 shows that if the peak force is 0.3, just below the minimum force to leave the galaxy, the momentum transfer becomes somewhat

enhanced, which pushes the particle into oscillations that approach the escape conditions.

This behaviour is characteristic for the test particle models for galaxies, which are presented in Section 2.3.1: While the stripped gas elements always absorb all the available momentum, gas parcels that would remain gravitationally bound receive their full share only for very short pulses, in accordance with the short pulse limit. At longer pulses they receive a progressively lower fraction. For pulse durations longer than about 200 Myr for a Milky Way type galaxy the momentum efficiency for all bound gas parcels nearly vanishes. This also reduces the fraction of gas which is kicked out of the disc and would later be reaccreted. Thus, in long pulses the gas disc is divided in an outer part escaping and an inner part remaining near the disc plane, without any intermediate part of reaccretable gas.

APPENDIX C: PARAMETERS OF H I DISTRIBUTION IN GALAXIES

The initial distribution of the gas in a galaxy is a very important parameter that influences how much gas can be removed from a galaxy subjected to a given ram pressure. It is impracticable or impossible to infer on the initial state of the gas disc in individual galaxies in our sample, which differ substantially in both their present gas disc and their basic parameters, such as size and rotation speed. However, we can use these data to deduce which general properties the unperturbed gas discs must have had. This section shows that reasonable assumptions of the HI radial scale and the ratio of initial H I radius and optical radius lead to satisfactory reproduction of the data.

The galaxies in the entire sample are shown in Fig. C1 as a relation between H I mass and optical radius. Among the galaxies with radii larger than about 5 kpc, there are several objects that have been studied in detail. The H I maps from VIVA allow us to distinguish different morphological features, such as tails and extensions of the H I disc which signify ongoing stripping, and well-truncated HI discs that may be taken as characteristic for stripping in the past. The galaxies of the sequence of Vollmer (2009), which appear to be at maximum ram pressure or quite close to it, have loci near the line for deficiency 1. Galaxies with one-sided tails from the H I disc (Chung et al. 2007) are positioned more closely to the line which corresponds to zero deficiency, thus indicating that they are at an early stage of stripping. Objects whose H I maps (from VIVA) show a well-truncated H I disc without any extending plume are found to be highly deficient. NGC 4388 and NGC 4569 also belong to this class. Galaxies whose HI diameter is larger than the optical diameter, like normal spirals, have negative deficiencies. In the figure, we mark and label only a few representative objects. NGC 4254 and NGC 4532 are non-deficient, but also have extensions of the HI disc.

Most objects smaller than about 5 kpc are irregular galaxies, for which more detailed informations are not available, such as HI maps. It is quite remarkable that they also follow the trend of the larger galaxies.

Fig. C1 shows that the sample galaxies follow rather well a quadratic dependence of the H I mass and optical radius. VIVA adopts for the formula to compute deficiencies a quadratic mass–diameter relation for normal galaxies, with a corresponding constant HI surface density of 8.3 $M_{\odot}pc^{-2}$ (as averaged over the optical radius). In this paper, we use the formula by Gavazzi et al. (2013) which also takes into account that the observed mass–diameter relation deviates from a simple quadratic dependence:

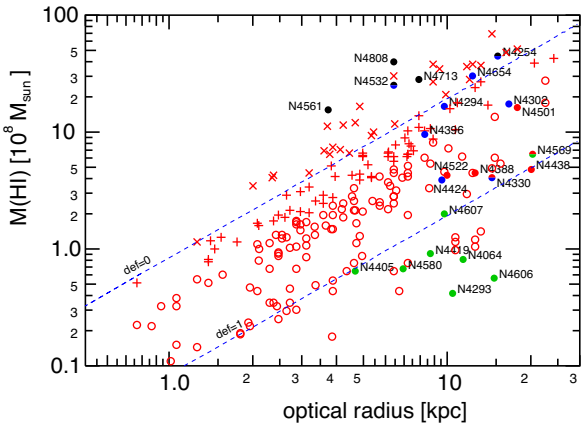

Figure C1. H I masses of galaxies in the Virgo cluster as a function of the optical radius (data from GoldMine). Black dots indicate several examples for non-deficient galaxies, red dots mark the sequence of stripped objects (Vollmer 2009), blue dots are galaxies with one-sided H I tails (Chung et al. 2007), and green dots are galaxies with clearly truncated H I discs, as found by inspection of HI maps in VIVA. Open circles are H I-deficient galaxies ($def > 0.3$), plus signs mark low-deficiency objects ($def < 0.3$), and X-signs are non-deficient objects ($def < 0$), based on the formula of Gavazzi et al. (2013) for deficiency. Two blue lines indicate the deficiencies of 0 and 1.

$$\mathrm{def} = 7.51 - \log_{10}(M_{\mathrm{H\,I}}) + 0.68 \times \log_{10}(d^2) \qquad \text{(C1)}$$

with the optical diameter d in kpc. The two relations for zero deficiency coincide for an optical radius of about 6 kpc. Thus, the choice of the formula to compute deficiencies is not overly critical. Both formulae give very similar results for normally sized galaxies; VIVA's formula gives larger deficiencies at very large objects, and smaller values for dwarf galaxies.

In most hydrodynamical and SPH simulations, the gas in the disc is treated as a continuous single-phase medium, whose surface density decreases outwards. Our analytical considerations are also based on this assumption. Since the maximum restoring force decreases outwardly as well, for a given ram pressure the gas beyond a certain 'stripping radius' is removed. The increase of the ram pressure during the flight of a galaxy towards the cluster interior thus causes a progressively stronger truncation of the gas disc, but leaves the interior of the remaining disc unaffected. Thus, one expects that the remnant disc preserves the properties of the inner unperturbed galactic gas disc.

VIVA gives two H I diameters: the isophotal one and the effective one, which are compared in Fig. C2. The ratio of the two radii is an indicator for extraplanar H I or tails, as non-deficient galaxies have $R_{\mathrm{eff}} \approx 0.7 \times R_{ISO}$, but galaxies like NGC 4522 with an extensive extraplanar H I plume have $R_{\mathrm{eff}} > R_{\mathrm{ISO}}$. The non-deficient NGC 4254 appears as a very odd object with $R_{\mathrm{eff}} \approx 30 \times R_{\mathrm{ISO}}$, whose isophotal diameter is given as an exceptionally low value of 0.15 arcmin, obviously a typo. We take the R_{eff} for the H I radius of this object.

The isophotal diameter uses a threshold of 1 $M_{\odot}\,pc^{-2}$ for the surface density. As this value can be expected to give a reliable measure for the extent of H I gas both in well-truncated discs and in normal galaxies (cf. Bigiel & Blitz 2012), we shall take the isophotal radius as the outer HI radius, keeping in mind that objects with substantial extraplanar gas can be misrepresented.

The dependence of the ratio of H I and optical radius on deficiency, depicted in Fig. C3, can be used to constrain the size of the initial H I

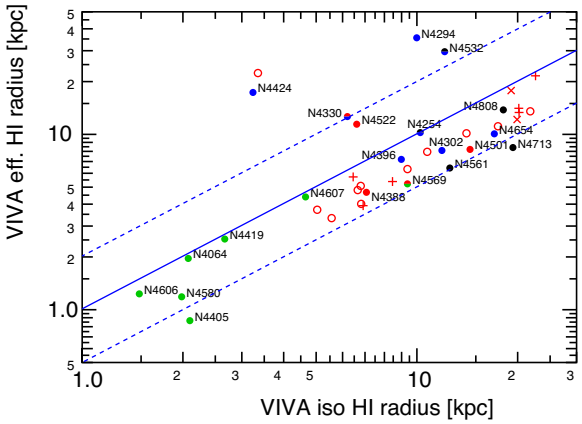

Figure C2. Comparison of the H I radii from VIVA: effective diameters $D_{\rm H\,I}^{\rm eff}$ contain 50 per cent of the total flux and isophotal diameters $D_{\rm H\,I}^{\rm ISO}$, where the azimuthally averaged HI surface density drops to 1 $M_\odot$ pc^{-2}. Symbols are as in Fig. C1. The full blue line indicates equality of the radii; the dashed lines a factor of 2 in either sense.

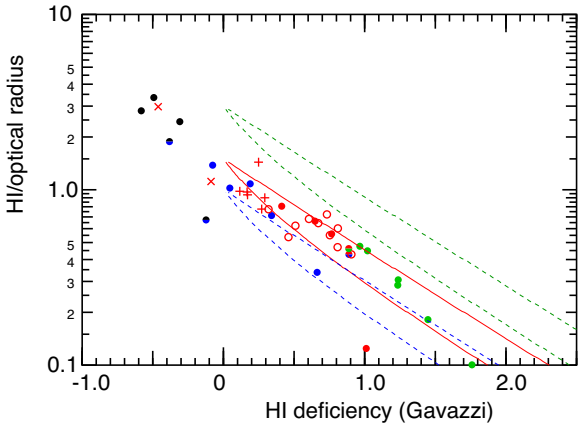

Figure C3. The ratio of the isophotal H I radius (from VIVA) and the optical radius (from GoldMine) of galaxies in the Virgo cluster as a function of H I deficiency (Gavazzi et al. 2013). Symbols are as in Fig. C1. The curves are the expected relations for exponential H I discs with the ratio of radial scale R and initial H I outer radius $r_{\rm max}$ of the disc $R/r_{\rm max} = 5$ and 0.5 (from top to bottom) and for the ratio $r_{\rm max}/r_{\rm opt}$ of 1 (blue), 1.5 (red), and 3 (green).

disc. The data are well reproduced, if one assumes that the HI radial scale is close to the optical radius, and if the initial H I radius is about 1.5 times the optical radius. This value agrees well with the results of Broeils & Rhee (1997) from large undisturbed field galaxies that suggest a value of 1.7. For our analyses, we shall adopt that the initial HI disc is a Miyamoto–Nagai disc with radial scale equal to the optical radius and is truncated at an outer radius 1.5 times the optical radius.

The mean H I surface density computed from the H I mass and the isophotal radius shows a remarkably small variation among the objects, as seen in Fig. C4. Most galaxies have mean surface densities around 4 $M_\odot$ pc^{-2}. Although Fig. C4 does not show a strong dependence of the average H I surface density on deficiency, one notes that the highly deficient objects with well-truncated H I discs have slightly higher surface densities than non-deficient galaxies. As in both types of objects, the isophotal diameters represent the true extent of the HI gas, this difference in mean surface density yields another constraint on the radial scale of the H I distribution:

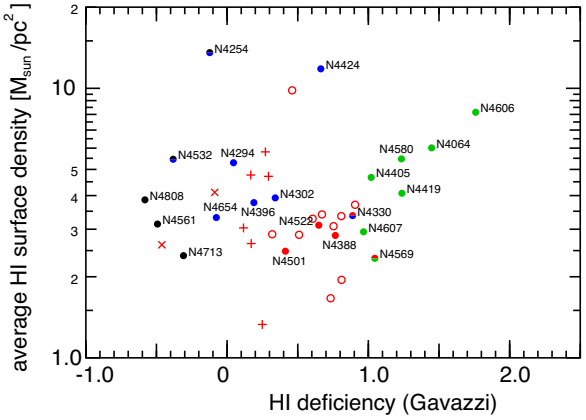

Figure C4. The mean H I surface density of galaxies in the Virgo cluster, computed from measured HI mass (GoldMine) and the isophotal H I diameters $D_{\rm H\,I}^{\rm ISO}$ (VIVA), within which the azimuthally averaged H I surface density exceeds 1 $M_\odot$ pc^{-2}, as a function of H I deficiency (Gavazzi et al. 2013). Symbols are as in Fig. C1.

The mean surface density of a disc with exponential profile, central density of 10 $M_\odot$ pc^{-2}, and outer radius of 15 kpc is 5.3 or 3.9 $M_\odot$ pc^{-2} for radial scales of 15 and 10 kpc, respectively. When truncated to deficiency 2, the mean surface density is close to the central value. Thus, our assumption that the H I radial scale is equal to the optical radius reproduces the weak trend seen in Fig. C4. The initial central density would then be taken from NGC 4606 as close to 8 $M_\odot$ pc^{-2}.

APPENDIX D: COMPARISON WITH VOLLMER'S MODELLINGS

Vollmer et al. (2001) and subsequent works have modelled in detail a number of VIVA sample galaxies. Since these objects serve here as a kind of calibration set, it is worthwhile to ascertain to what extent our analytical approach is able to reproduce also these models. The ISM was treated as a population of H I clouds with different masses but fixed column density, and a sticky-particle algorithm was used to model the interaction by inelastic collisions that give rise to fragmentation, coalescence, and mass exchange of clouds. Furthermore, to account for clouds becoming denser closer to the galaxy's centre, an enhancement factor was applied in the restoring force, as in equation (27).

We compute from the H I deficiency the stripping radius, assuming a Miyamoto–Nagai disc, and then use equation (27) with the fixed value for the gas surface density of $\Sigma_{\rm H} = 7.75$ $M_\odot$ pc^{-2} and a fixed scale length of $R_0 = 2$ kpc, as used by Vollmer et al. (2001) to compute the required ram pressure. This is done for models M, N, O, and P of Vollmer et al. (2001), for which the actual gas density profiles are not given, but we find that with a radial scale of 20 kpc for the Miyamoto–Nagai gas disc we recover the maximum ram pressures by better than 6 per cent, and the stripping radii within a factor of 1.5.

With this prescription we now analyse the data of our full GoldMine sample, assuming again that the HI disc has an initial outer radius of 1.5 times the optical radius and follows a Miyamoto–Nagai profile with radial scale equal to the optical radius (see Appendix C for details). The results are shown in Fig. D1: Because of the higher value for the H I column density for all objects, the required ram pressures needed to account for the deficiencies are higher than in Fig. 15, typically by about a factor of 3, which would be

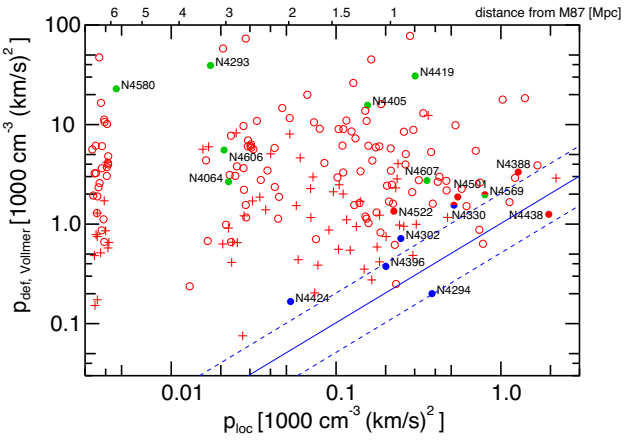

Figure D1. Similar to Fig. 15, but using approach of Vollmer et al. (2001) that represents the ISM as a population of HI clouds of equal column density.

still acceptable in view of the overall uncertainties for the pressure estimates.

Although the required ram pressures are already higher than estimated from Fig. 15, they still are systematically below the values used by Vollmer in his individual modellings. For example, NGC 4522 needs 1350 cm^{-3}(km s^{-1})^2 (or 800 when R_0 is scaled with the optical radius (equation 23) instead of 2000 (Vollmer et al. 2006). NGC 4388 requires 3300 (or 2600) instead of 5000 (Vollmer & Huchtmeier 2003), but Damas-Segovia et al. (2016) report that a value three times lower is needed, i.e. 1700 cm^{-3}(km s^{-1})^2. Figure 5 of Vollmer (2009) also shows that for most of the galaxies the maximum ram pressure is higher (factor of 2 and more) than estimated from the local ICM density. While this factor is still acceptable within the overall uncertainties of the data, a possible explanation lies with the assumed gas distribution. The modellings unfortunately do not provide information about the initial or the current gas density profile, such as radial scale and initial outer radius. Had we adopted radial scales substantially smaller (about one half) than the optical radius, we would get indeed required ram pressures as high as the published values.

APPENDIX E: THE CATALOGUE

Table E1. Virgo galaxies which undergo stripping at present, with $p_{\rm def} < 2p_{\rm loc}$, sorted in descending order of H I deficiency. The columns are H I deficiency, linear distance from M87 (Mpc), optical radius (kpc), HI isophotal radius (kpc) (from VIVA, when available), rotational velocity (km s^{-1}), local ram pressure (1000 cm^{-3}(km s^{-1})^2), maximum ram pressure estimated by the centrifugal acceleration at the observed HI radius (1000 cm^{-3}(km s^{-1})^2), and the ram pressure needed to produce the current HI deficiency (1000 cm^{-3}(km s^{-1})^2).

Name	*def*	*d*	$r_{\rm opt}$	$r_{\rm H\,I,iso}$	$v_{\rm rot}$	$p_{\rm loc}$	$p_{\rm max}$	$p_{\rm def}$
NGC 4438	1.01	0.29	20.1	–	134.1	1.95	–	0.92
IC3611	0.98	0.66	4.4	–	37.6	0.47	–	0.79
NGC 4330	0.89	0.63	14.5	6.2	121.8	0.52	0.32	0.86
NGC 4413	0.8	0.32	7.2	–	99.1	1.67	–	1.3
NGC 4388	0.77	0.37	12.6	7.1	182.3	1.27	0.59	1.59
NGC 4424	0.66	1.98	9.6	3.2	34.5	0.05	0.07	0.06
NGC 4522	0.65	0.98	10.0	6.6	105.7	0.22	1.85	0.52
IC3476	0.63	0.51	6.4	–	91.1	0.75	–	0.74
NGC 4402	0.61	0.4	9.8	6.7	122.5	1.13	0.28	0.62
NGC 4540	0.57	0.98	6.4	–	78.3	0.22	–	0.44
IC3258	0.57	0.51	6.4	–	57.8	0.74	–	0.24
IC3239	0.56	0.59	3.1	–	45.6	0.58	–	0.48
VCC1605	0.51	0.66	2.5	–	43.5	0.47	–	0.54
VCC328	0.49	0.85	2.5	–	39.1	0.29	–	0.41
IC3583	0.45	0.5	6.9	–	65.1	0.78	–	0.18
IC797	0.42	0.81	4.2	–	80.5	0.32	–	0.57
IC3365	0.42	1.07	6.1	–	68.0	0.19	–	0.21
IC3059	0.41	1.19	4.6	–	60.0	0.15	–	0.26
NGC 4501	0.41	0.61	17.9	14.4	296.0	0.55	0.43	0.68
IC3311	0.38	0.38	3.6	–	75.3	1.22	–	0.55
IC3414	0.36	1.67	4.5	–	49.4	0.08	–	0.15
IC3142	0.36	0.97	3.1	–	31.3	0.23	–	0.11
IC3453	0.35	0.73	3.0	–	48.8	0.39	–	0.28
NGC 4302	0.34	0.93	16.7	11.9	187.6	0.25	0.25	0.23
IC3105	0.34	0.96	6.4	–	46.1	0.23	–	0.07
VCC1644	0.32	0.57	2.4	–	41.0	0.62	–	0.25
NGC 4321	0.32	1.17	22.5	17.5	268.8	0.16	0.27	0.27
NGC 4595	0.29	1.08	5.3	–	90.4	0.18	–	0.29
VCC512	0.28	0.66	3.6	–	56.5	0.47	–	0.21
NGC 4298	0.27	0.94	8.9	6.9	148.8	0.24	0.37	0.31
VCC87	0.21	1.53	3.6	–	55.9	0.09	–	0.15
NGC 4633	0.2	1.03	6.1	–	99.9	0.2	–	0.19
NGC 4396	0.19	1.03	8.3	9.0	99.0	0.2	0.08	0.11
NGC 4470	0.18	1.36	4.5	–	88.5	0.12	–	0.23
IC3446	0.18	0.27	2.7	–	80.9	2.16	–	0.43
NGC 4192	0.17	1.43	24.2	22.6	234.7	0.1	0.12	0.1
NGC 4222	0.17	1.08	8.7	8.5	113.0	0.18	0.13	0.12
IC3562	0.16	0.83	2.1	–	38.2	0.31	–	0.13
VCC1437	0.14	0.96	1.5	–	43.2	0.23	–	0.28
NGC 4498	0.12	1.33	7.0	–	116.1	0.12	–	0.14
NGC 4535	0.12	1.27	20.6	20.2	297.9	0.13	0.22	0.15
NGC 4639	0.1	0.91	7.9	–	176.3	0.26	–	0.23
NGC 4688	0.08	2.69	10.9	–	63.1	0.03	–	0.02
IC3074	0.08	1.2	7.2	–	104.0	0.15	–	0.08
VCC1726	0.07	1.65	3.2	–	45.0	0.08	–	0.06
IC3742	0.07	1.1	5.0	–	95.4	0.18	–	0.12
NGC 4294	0.05	0.74	9.8	10.0	101.1	0.38	0.08	0.04
NGC 4206	0.04	1.14	12.6	–	137.5	0.16	–	0.04
IC3591	0.0	1.68	3.8	–	49.9	0.07	–	0.03
NGC 4523	0.0	0.85	7.9	–	148.5	0.29	–	0.08

Table E2. Like Table E1, but for galaxies that had undergone stripping in the past (with $p_{def} > 2p_{loc}$).

Name	*def*	*d*	r_{opt}	$r_{H\,I,iso}$	v_{rot}	p_{loc}	p_{max}	p_{def}
NGC 4606	1.76	3.03	14.8	1.5	76.7	0.02	0.67	3.75
NGC 4293	1.69	3.3	10.5	–	163.7	0.02	–	24.8
IC796	1.47	1.2	3.9	–	56.6	0.15	–	9.02
NGC 4064	1.45	2.95	11.4	2.1	58.8	0.02	0.32	1.56
NGC 4309	1.4	6.42	6.7	–	164.3	0.0	–	26.54
NGC 4313	1.4	0.62	12.6	–	131.8	0.53	–	5.75
NGC 4312	1.34	1.11	12.6	–	109.6	0.17	–	3.51
NGC 4586	1.33	2.46	10.7	–	127.6	0.03	–	6.02
VCC1623	1.32	1.3	1.8	–	54.4	0.13	–	19.37
VCC1970	1.3	1.15	1.8	–	71.1	0.16	–	33.23
NGC 4307	1.29	6.21	13.2	–	162.5	0.0	–	6.29
NGC 4445	1.26	6.12	10.7	–	133.5	0.0	–	5.5
NGC 4419	1.24	0.84	8.7	2.7	195.7	0.3	3.01	15.3
NGC 4580	1.23	5.81	6.9	2.0	138.5	0.0	2.39	10.92
NGC 4356	1.22	6.23	10.7	–	147.5	0.0	–	5.95
IC3718	1.21	1.01	6.4	–	36.2	0.21	–	0.79
IC3392	1.21	0.79	7.2	–	111.0	0.34	–	6.08
IC3374	1.08	6.08	3.9	–	42.2	0.0	–	1.69
IC3077	1.06	1.23	2.9	–	31.9	0.14	–	1.48
VCC517	1.05	2.26	2.5	–	170.2	0.04	–	52.68
NGC 4569	1.05	0.49	26.5	9.4	215.9	0.8	0.49	1.69
IC3520	1.02	0.43	2.6	–	71.4	1.03	–	7.45
NGC 4405	1.02	1.17	4.7	2.1	102.3	0.16	1.35	5.95
VCC513	1.0	3.05	1.8	–	102.5	0.02	–	26.84
IC3412	0.99	6.08	3.9	–	50.3	0.0	–	1.77
VCC1459	0.99	2.9	1.8	–	37.7	0.02	–	3.47
VCC1784	0.97	1.14	2.0	–	30.0	0.17	–	1.85
VCC1465	0.97	2.68	2.7	–	56.1	0.03	–	3.71
NGC 4607	0.97	0.77	9.8	4.7	91.5	0.36	0.3	1.21
NGC 4641	0.95	0.9	3.4	–	42.9	0.26	–	1.41
IC800	0.94	0.91	4.6	–	80.6	0.26	–	2.96
IC3716	0.94	1.63	1.9	–	44.3	0.08	–	3.63
VCC1013	0.94	6.13	2.4	–	33.3	0.0	–	1.41
IC3521	0.92	1.58	4.9	–	60.8	0.08	–	1.41
NGC 4380	0.91	6.1	11.8	5.0	151.3	0.0	0.7	1.98
VCC1744	0.9	0.85	1.3	–	34.7	0.29	–	3.88
VCC479	0.89	6.3	2.4	–	43.3	0.0	–	2.11
VCC1821	0.89	1.77	1.0	–	46.0	0.07	–	9.54
VCC1597	0.87	2.09	2.3	–	67.0	0.05	–	5.0
IC3483	0.85	0.35	2.7	–	86.1	1.4	–	5.85
NGC 4579	0.81	0.53	15.6	9.4	278.6	0.7	0.86	3.05
NGC 4689	0.81	1.29	14.5	6.8	137.3	0.13	0.36	0.83
VCC514	0.79	6.24	4.7	–	35.4	0.0	–	0.32
VCC1574	0.78	0.87	1.1	–	101.8	0.28	–	29.53
NGC 4450	0.75	3.4	12.3	6.8	207.2	0.02	0.82	2.03
NGC 4287	0.74	6.66	4.9	–	86.0	0.0	–	1.55
NGC 4548	0.73	0.71	14.8	10.7	206.4	0.41	0.36	1.39
IC3517	0.71	1.0	2.9	–	44.4	0.22	–	0.87
VCC1208	0.71	2.61	2.1	–	49.5	0.03	–	1.86
NGC 4351	0.67	3.35	8.6	5.6	60.6	0.02	0.09	0.23
VCC1931	0.66	0.9	3.1	–	60.7	0.26	–	1.2
NGC 4544	0.65	2.8	6.1	–	101.0	0.03	–	1.06
VCC453	0.64	0.74	2.0	–	44.1	0.38	–	1.3
NGC 4353	0.62	6.31	4.7	–	79.1	0.0	–	0.88
IC3094	0.58	1.07	2.3	–	92.5	0.19	–	3.49
VCC1048	0.58	6.58	5.7	–	96.0	0.0	–	0.83
NGC 4571	0.56	0.7	11.3	–	209.2	0.42	–	1.23
VCC297	0.55	6.53	3.9	–	67.5	0.0	–	0.7
IC3259	0.55	6.39	5.7	–	89.8	0.0	–	0.65
NGC 4237	0.55	1.31	5.0	–	140.9	0.12	–	2.01
VCC1725	0.54	1.24	3.8	–	47.7	0.14	–	0.35
NGC 4451	0.53	6.13	6.6	–	117.2	0.0	–	0.84

Table E3. Table E2, continued.

Name	*def*	*d*	r_{opt}	$r_{H\,I,iso}$	v_{rot}	p_{loc}	p_{max}	p_{def}
VCC1529	0.52	2.63	2.9	–	32.0	0.03	–	0.23
VCC568	0.51	6.54	3.3	–	85.0	0.0	–	1.24
NGC 4216	0.51	1.1	22.5	14.1	260.7	0.18	0.38	0.51
NGC 4416	0.5	1.36	5.4	–	186.2	0.12	–	2.66
VCC1758	0.5	1.44	4.2	–	75.0	0.1	–	0.64
IC3049	0.5	1.39	3.1	–	59.3	0.11	–	0.65
VCC1789	0.5	2.3	2.7	–	54.0	0.04	–	0.68
NGC 4412	0.5	2.52	4.7	–	115.3	0.03	–	1.27
VCC1596	0.49	1.0	0.9	–	30.8	0.21	–	1.41
NGC 4591	0.49	1.99	4.6	–	165.0	0.05	–	2.58
NGC 4502	0.49	1.28	3.7	–	104.3	0.13	–	1.47
IC3066	0.48	1.17	2.5	–	67.6	0.16	–	1.18
NGC 4324	0.47	2.19	8.7	–	160.4	0.04	–	0.79
VCC859	0.47	2.68	7.2	–	160.0	0.03	–	1.07
NGC 4694	0.46	3.75	6.2	3.4	34.7	0.01	0.07	0.06
IC3471	0.46	1.08	2.1	–	60.8	0.18	–	1.13
VCC168	0.45	1.18	1.1	–	50.6	0.15	–	2.28
VCC324	0.44	2.67	3.3	–	56.1	0.03	–	0.42
NGC 4634	0.44	1.03	7.2	–	137.5	0.2	–	0.71
VCC415	0.43	6.47	3.9	–	61.3	0.0	–	0.38
NGC 4430	0.43	6.49	10.1	–	150.9	0.0	–	0.47
VCC1750	0.41	1.69	0.8	–	41.7	0.07	–	2.36
NGC 4466	0.4	1.4	3.0	–	88.6	0.11	–	1.11
VCC468	0.4	2.56	1.4	–	47.4	0.03	–	1.11
VCC130	0.4	1.39	1.6	–	63.0	0.11	–	1.61
VCC1060	0.39	2.82	2.6	–	56.8	0.02	–	0.54
NGC 4343	0.39	6.42	8.3	–	173.3	0.0	–	0.75
NGC 4866	0.38	2.13	14.8	–	271.0	0.05	–	0.69
IC3298	0.38	1.43	2.5	–	95.9	0.1	–	1.56
VCC404	0.38	2.55	4.2	–	127.5	0.03	–	1.2
IC3322	0.38	6.33	7.2	–	91.6	0.0	–	0.25
VCC467	0.38	2.65	1.1	–	140.8	0.03	–	13.71
VCC628	0.37	6.33	0.9	–	61.8	0.0	–	3.2
NGC 4533	0.37	3.0	6.4	–	86.5	0.02	–	0.26
VCC1572	0.36	2.93	2.3	–	53.1	0.02	–	0.52
VCC329	0.36	6.63	2.1	–	39.0	0.0	–	0.32
VCC1918	0.35	2.15	2.5	–	35.5	0.04	–	0.19
VCC888	0.35	6.23	3.9	–	41.2	0.0	–	0.13
VCC1507	0.33	2.56	2.9	–	96.7	0.03	–	1.08
NGC 4630	0.33	2.64	5.7	–	101.9	0.03	–	0.38
VCC772	0.32	2.4	1.3	–	33.0	0.03	–	0.46
VCC693	0.31	2.2	2.9	–	95.7	0.04	–	0.98
VCC741	0.31	2.61	2.1	–	72.6	0.03	–	0.95
IC3099	0.3	0.99	4.6	–	105.5	0.22	–	0.53
VCC1266	0.3	2.9	2.9	–	32.8	0.02	–	0.11
NGC 4212	0.3	1.18	8.9	–	152.3	0.15	–	0.37
NGC 4289	0.3	2.67	10.7	–	187.5	0.03	–	0.41
VCC1685	0.3	2.79	5.3	–	64.5	0.03	–	0.15
VCC1011	0.29	1.43	3.2	–	71.5	0.1	–	0.43
NGC 4772	0.29	3.46	7.2	6.5	272.3	0.02	1.28	1.64
IC3229	0.28	6.47	3.9	–	65.1	0.0	–	0.24
IC3225	0.28	6.47	7.2	–	103.1	0.0	–	0.22
IC3474	0.28	2.89	7.2	–	76.5	0.02	–	0.12
NGC 4378	0.27	2.25	7.6	–	284.3	0.04	–	1.52
NGC 4647	0.27	0.95	6.4	–	178.6	0.23	–	0.76
NGC 4207	0.26	1.39	4.8	–	108.9	0.11	–	0.44
NGC 4698	0.25	1.73	14.0	20.2	236.6	0.07	0.09	0.34
VCC826	0.24	3.06	3.0	–	36.8	0.02	–	0.1
IC3061	0.23	1.24	6.4	–	149.5	0.14	–	0.45
VCC1257	0.23	1.49	3.4	–	79.1	0.1	–	0.36
NGC 4758	0.22	1.88	7.4	–	90.2	0.06	–	0.13
VCC675	0.22	2.81	1.4	–	69.0	0.02	–	1.15
VCC952	0.22	6.1	2.6	–	32.3	0.0	–	0.09
VCC509	0.21	6.52	4.9	–	75.6	0.0	–	0.17

Table E4. Table E2 (continued).

Name	*def*	*d*	r_{opt}	$r_{H\,I,iso}$	v_{rot}	p_{loc}	p_{max}	p_{def}
VCC334	0.2	0.95	1.4	–	49.8	0.24	–	0.55
NGC 4390	0.19	6.07	7.3	–	114.8	0.0	–	0.18
VCC1933	0.19	1.73	1.8	–	46.2	0.07	–	0.3
VCC740	0.19	6.23	2.4	–	53.2	0.0	–	0.24
NGC 4779	0.17	1.86	5.2	–	217.7	0.06	–	1.04
VCC1156	0.17	2.87	6.1	–	99.8	0.02	–	0.16
VCC1468	0.16	2.32	2.5	–	52.5	0.04	–	0.19
NGC 4376	0.16	6.59	6.2	–	87.3	0.0	–	0.12
NGC 4316	0.16	6.18	8.3	–	157.5	0.0	–	0.24
IC3268	0.14	6.47	6.5	–	58.9	0.0	–	0.04
VCC459	0.13	1.7	2.1	–	68.9	0.07	–	0.38
NGC 4799	0.11	3.34	4.0	–	207.1	0.02	–	1.06
NGC 4423	0.09	6.55	10.2	–	85.0	0.0	–	0.03
NGC 4420	0.08	2.95	5.0	–	115.7	0.02	–	0.18
VCC1141	0.07	6.12	1.5	–	69.1	0.0	–	0.44
NGC 4067	0.07	1.99	3.0	–	189.9	0.05	–	1.12
VCC410	0.05	0.76	0.8	–	70.3	0.36	–	1.24
VCC1873	0.05	1.9	1.4	–	40.5	0.06	–	0.15
NGC 4480	0.05	2.42	5.0	–	178.8	0.03	–	0.36
VCC737	0.03	2.53	2.6	–	85.0	0.03	–	0.21
VCC975	0.01	6.35	13.2	–	198.2	0.0	–	0.07

Table E5. Like Table E1, but for non-deficient galaxies.

Name	*def*	*d*	r_{opt}	$r_{H\,I,iso}$	v_{rot}	p_{loc}	p_{max}	p_{def}
VCC423	– 0.0	2.9	1.3	–	33.0	0.02	–	–
NGC 4635	– 0.02	2.39	4.5	–	110.3	0.04	–	–
IC3617	– 0.05	1.46	3.2	–	52.5	0.1	–	–
CGCG97067	– 0.05	3.88	6.5	–	107.6	0.01	–	–
IC3881	– 0.05	2.64	9.9	–	104.6	0.03	–	–
VCC827	– 0.06	6.37	12.0	–	140.5	0.0	–	–
IC3576	– 0.06	1.76	5.3	–	43.1	0.07	–	–
NGC 4654	– 0.08	0.97	12.3	17.0	165.8	0.23	0.07	–
NGC 4746	– 0.08	1.53	5.4	–	170.8	0.09	–	–
NGC 4536	– 0.09	3.04	17.9	19.9	194.6	0.02	0.1	–
IC3522	– 0.09	0.89	4.1	–	58.1	0.27	–	–
IC3371	– 0.1	0.52	3.8	–	78.0	0.73	–	–
NGC 4303	– 0.11	2.44	16.3	–	131.7	0.03	–	–
NGC 4254	– 0.12	1.05	15.2	10.2	271.4	0.19	0.92	–
NGC 4178	– 0.13	1.39	13.2	–	132.3	0.11	–	–
VCC848	– 0.15	6.57	3.9	–	137.3	0.0	–	–
VCC1581	– 0.16	1.83	3.6	–	83.9	0.06	–	–
NGC 4123	– 0.18	3.28	12.4	–	165.4	0.02	–	–
VCC1375	– 0.18	2.51	11.8	–	138.8	0.03	–	–
NGC 4186	– 0.19	1.44	2.3	–	75.0	0.1	–	–
VCC566	– 0.2	6.27	2.4	–	49.5	0.0	–	–
VCC1992	– 0.21	0.97	2.0	–	65.6	0.23	–	–
NGC 4519	– 0.22	1.13	8.9	–	119.7	0.17	–	–
NGC 4301	– 0.25	2.4	4.7	–	89.9	0.03	–	–
IC3356	– 0.29	0.38	4.2	–	40.1	1.24	–	–
NGC 4116	– 0.3	3.34	9.4	–	137.1	0.02	–	–
NGC 4713	– 0.31	2.53	7.9	19.4	109.5	0.03	0.02	–
NGC 4527	– 0.34	2.9	14.5	–	193.8	0.02	–	–
NGC 4765	– 0.36	2.87	3.7	–	54.9	0.02	–	–
VCC1091	– 0.37	6.18	4.9	–	90.8	0.0	–	–
NGC 4701	– 0.37	2.99	8.9	–	155.7	0.02	–	–
NGC 4532	– 0.38	1.78	6.4	12.1	85.4	0.07	0.04	–
NGC 4383	– 0.46	1.27	6.4	19.1	123.6	0.13	0.02	–
NGC 4561	– 0.49	2.09	3.7	12.5	164.9	0.05	0.06	–
NGC 4808	– 0.58	3.02	6.4	18.1	146.4	0.02	0.05	–

This paper has been typeset from a TEX/LATEX file prepared by the author.